Quantitative Finance, 2017
Vol. 17, No. 5, 657–675, http://dx.doi.org/10.1080/14697688.2016.1231417

Routledge
Taylor & Francis Group

Birth or burst of financial bubbles: which one is easier to diagnose?

G. DEMOS*† and D. SORNETTE‡

†Department of Management, Technology and Economics, ETH Zürich, Zürich, Switzerland
‡Swiss Finance Institute, 40, Boulevard du Pont-d' Arve, 1211 Geneva 4, Switzerland

(*Received 7 December 2015; accepted 25 August 2016; published online 23 November 2016*)

1. Introduction

Financial bubbles and their subsequent crashes provide arguably the most visible departures from well-functioning efficient markets. There is an extensive literature (see e.g. the reviews Kaizoji and Sornette 2010, Xiong 2013) on the causes of bubbles as well as the reasons for bubbles to be sustained over surprising long periods of time. One prominent question is: Why are not arbitragers quelling bubbles in the same way that investment opportunities based on market imperfections tend to be removed by arbitrage? Among many arguments advanced in the literature, we here focus on the one suggested by Abreu and Brunnermeier (2003). In the authors' set-up, market participants become aware about the mispricing developing during the bubble in a disorganized fashion, one after another. Thus, opinions differ about the date when the bubble really started, preventing a coordinated arbitrage that would have put an end to the burgeoning bubble.

We question this view and mechanism. Indeed, from informal private exchanges with a large number of practitioners during massive bubbles (such as the dot-com bubble that terminated in 2000), it appears that the existence of a bubble permeates rather early in to the consciousness of professionals. For instance, hedge-funds tend to correctly diagnose bubbles in their early stages (Gurkaynak 2008). Think for instance of the famous 'irrational exuberance' quip of Federal Reserve chairman, Alan Greenspan, issued on 5 December 1996, more than three years before the bubble finally burst. One could have thought that such a strong statement from such a respected authority (at the time) would have synchronized the attention of arbitragers, leading to the demise of this bubble. In fact, after a minor volatility spike lasting no more than a few days following Greenspan's statement, the markets roared unabated to new highs, with the years of 1998 and 1999 enjoying a sky-rocketing cumulative return of more than 1100% for the technology sector. This suggests that bubbles do not persist and flourish because of a lack of general perception of their presence at early times. Rather than shorting the bubble, it is in the interest of investors to 'surf' it as long as it lasts (Brunnermeier and Nagel 2004), given that the gains are so extraordinary that they typically attract less and less sophisticated investors as well as generally less well-informed foreigners, further fuelling the ascent of the bubble (Shleifer 2000, Sornette 2003). Moreover, it often happens that value investors opportunistically transform into momentum followers during bubble regimes.

Rather than the beginning of bubbles, we argue that it is their ends that are devilishly difficult to forecast with any useful accuracy. As Keynes famously commented: 'The market can stay irrational longer than you can stay solvent.' And Greenspan's statement mentioned above also illustrates the discrepancy between an early diagnostic and the much delayed conclusion of the bubble. The contribution of the present article is to propose a methodology to quantify these intuitions. We put numbers on how precise can be the early diagnostic of a nucleating bubble and the estimation of its lifetime. For this, we use the log-periodic power law singularity (LPPLS) model (Johansen *et al.* 2000, Sornette 2003) to represent bubble regimes. We endogenize t_1 as a parameter to calibrate and

*Corresponding author. Email: gdemos@ethz.ch

estimate the LPPLS model on synthetic time series generated by the LPPLS model with noise and on eight historical bubble cases. In order to determine the uncertainties of the calibrated parameters we calculate the eigenvalues and eigenvectors of the Fisher Information Matrix defined from the cost function of the calibration exercise, following , Bree *et al.* (2013), Transtrum *et al.* (2011) and Machta *et al.* (2013). Comparing the eigenvalues and the parameters that contribute to the corresponding eigenvalues, we can estimate the 'rigid' parameters vs. the 'sloppy' ones, the later being characterized by very small eigenvalues so that the cost function is essentially insensitive to their specific values, making them impossible to determine precisely. We find that the eigenvalues of the Hessian matrix approximated at the best-fit parameters whose eigenvectors are dominated by t_1 tend to be three orders of magnitude larger than those controlled by t_c. As a rough estimate, this implies that the errors on t_c are about 30 times larger that on t_1. The determination of the end of the bubble is thus much more difficult that its beginning. This suggests that the lack of knowledge regarding the end of the bubble t_c should play a more important role on asset price inflation than the lack of agents consensus about t_1.

The article is structured as follows. Section 2 presents the LPPLS model (Johansen *et al.* 2000) alongside an initial result of the sloppy-rigid analysis performed on synthetic data. We then extend the application of the method to real-world data in section 3 and conclude in section 4.

2. The LPPLS model

2.1. Brief review of the literature on bubbles

The weak *efficient-market-hypothesis* stresses that prices should reflect all available information at a given time (Samuelson 1965) while any mispricing should be promptly arbitraged by market makers. In reality, many anomalies seem to persist, the bubble phenomenon being arguably the prominent one. Financial bubbles are often considered a product of coordinating interactions at the microscopic level between economic agents, leading to the observed price trajectory of an asset to decouple from its underlying fundamental value (Kindleberger 1978, Sornette 2003). Why do bubbles start and why they persist are subjects of much controversy (Kindleberger 1978, Xiong 2013, Sornette 2014).

Minsky (1974) suggested the importance of loose monetary policy in enhancing the price decoupling during bubbles. Innovations, both financial and technological, also tend to be associated with beginnings of bubbles (Kindleberger 1978, Shiller 1981). Moreover, the task of correctly pricing the fundamental value of a given firm or asset involves much uncertainty, due to inherent sensitivity of the method of discounting future dividends or earnings through time (Gurkaynak 2008).

Financial bubbles were shown to be persistent even in the presence of rational expectation agents (Blanchard and Watson 1982). The behavioural feedback-loop theory for example holds that higher present observable prices lead to higher expected price appreciation (Barberis *et al.* 1998, Shiller 2000). This resembles the resale option theory (Harrison and Kreps 1978). In this framework, rational agents are willing to pay more than their own expectation of the asset fundamental value because they expect to re-sell the asset in the future to a more optimistic agent, for a higher price. Hüsler *et al.* (2012) test these ideas quantitatively in a set of bubble experiments.

2.2. Presentation of the model

Building on this idea of positive feedbacks by imitation, the JLS model proposed by Johansen *et al.* (2000) and its extensions includes as a key ingredient the role played by herding behaviour in the formation of bubbles. Considering bubbles as a transient phenomenon, the existence of positive feedbacks between value investors and noise traders create a super-exponential growth of the price, decorated by deviations around the price growth in the form of oscillations that are periodic in the logarithm of the time to the burst of the bubble. When imitation reaches a certain threshold, the higher demand for the asset leads to the observable price to increase, bootstrapping on itself, and the market is governed by sentiment rather than some real underlying value (Sornette and Cauwels 2015). This process is intrinsically unsustainable and the mispricing ends at a critical time t_c, either smoothly into another regime or abruptly (crash). In short, in this set-up (as well as the one discussed above (Abreu and Brunnermeier 2003)), it is assumed that agents are fully aware of the mispricing.

In a bubble regime, the observed price trajectory of a given asset decouples from its intrinsic fundamental value (Kindleberger 1978, Sornette 2003). For a given fundamental value, the JLS model (Johansen *et al.* 2000) assumes that the logarithm of the observable asset price $p(t)$ follows

$$\frac{\mathrm{d}(p)}{p} = \mu(t)\mathrm{d}t + \sigma(t)\mathrm{d}W - k\mathrm{d}j, \qquad (1)$$

where $\mu(t)$ is the expected return, $\sigma(t)$ is the volatility, $\mathrm{d}W$ is the infinitesimal increment of a standard Wiener process and $\mathrm{d}j$ represents a discontinuous jump such that $j = n$ before and $j = n + 1$ after a crash occurs (where n is an integer). The parameter k quantifies the amplitude of a possible crash.

Two types of agents are considered: the first group consists in traders with rational expectations (Blanchard and Watson 1982), while the second one is characterized by noise traders with herding behaviour. The collective behaviour of the latter class of traders can destabilize asset prices. Johansen *et al.* (2000) propose that their behaviour can be mimicked by writing the $crash\,hazard\,rate$ under the following form

$$h(t) = \alpha(t_c - t)^{m-1}\left(1 + \beta\,\cos(\omega\,\ln(t_c - t) - \phi'\right), \qquad (2)$$

where α, β, ω and t_c are parameters. Equation (2) tells us that the risk of a crash resulting from herding behaviour is a sum of a power law singularity ($\alpha(t_c - t)^{m-1}$), which is decorated by large-scale amplitude oscillations that are periodic in the logarithm of the time to the singularity (or critical time) t_c. The power law singularity embodies the positive feedback mechanism associated with the herding behaviour of noise traders. The log-periodic oscillations represent the tension and competition between the two types of agents that tend to create deviations around the faster-than-exponential price growth as the market approaches a finite-time-singularity at t_c.

The no-arbitrage condition imposes that the excess return $\mu(t)$ during a bubble phase is proportional to the crash hazard rate given by equation (2). Indeed, setting $E[\mathrm{d}p] = 0$, and

assuming that no-crash has yet occurred ($\mathrm{d}j = 0$), this yields $\mu = kh(t)$, since $E[\mathrm{d}j] = h(t)\mathrm{d}t$ by definition of $h(t)$. By integration, we obtain the expected trajectory of the price logarithm during a bubbly trajectory, conditional on the crash not yet happening, as

$$E[\ln p(t)] = A + B|t_c - t|^m + C|t_c - t|^m \cos\big(\omega \ln|t_c - t| - \phi\big), \quad (3)$$

with $B = -k\alpha/m$ and $C = -k\alpha\beta/\sqrt{m^2+\omega^2}$. Note that the formula extends the price dynamics beyond t_c by replacing $t_c - t$ by $|t_c - t|$, which corresponds to assuming a symmetric behaviour of the average of the log-price around the singularity at t_c.

Bubble regimes are in general characterized by $0 < m < 1$ and $B < 0$. The first condition $m < 1$ writes that a singularity exists (the momentum of the expected log-price diverges at t_c for $m < 1$), while $m > 0$ ensures that the price remains finite at the critical time t_c. The second condition $B < 0$ expresses that the price is indeed growing super-exponentially towards t_c (for $0 < m < 1$).

2.3. Estimating the model

Filimonov and Sornette (2013) re-wrote expression (3) by expanding the term $C\cos[.]$ to replace the two parameters C and ϕ by two linear parameters $C_1 = C\cos\phi$ and $C_2 = C\sin\phi$. This representation reduces the complexity of the calibration of the LPPLS model through the reduction of the number of nonlinear (NL) parameters from 4 (m, ω, t_c, ϕ) to 3 (m, ω, t_c), while augmenting the set of linear parameters to 4 (A, B, C_1, C_2). In the present article, each fit was performed using the Levenberg–Marquardt algorithm (Marquardt 1962), with starting values for the nonlinear parameters obtained from a previous Nelder–Mead Simplex search method. Appendix 1 summarizes the two-step procedure used to determine first the four slaved linear parameters and then the three nonlinear parameters.

Previous calibrations of the JLS model have further shown the value of additional constraints imposed on the nonlinear parameters in order to remove spurious calibrations (false positive identification of bubbles) (Sornette and Johansen 2001, Jiang *et al*. 2010, Johansen and Sornette 2010, Geraskin and Fantazzini 2011).

(i) **exponent** $0.1 < m < 0.9$: This more stringent constraint than the one $(0 < m < 1)$ discussed above improves the power of discriminating bubbles by removing calibrations that select parameters too close from the bounds.

(ii) **angular log-periodic frequency** $6 < \omega < 13$: This condition ensures that the preferred scaling ratio $:= e^{\frac{2\pi}{\omega}}$ of the log-periodicity (Sornette 1998) is of the order of 2, as suggested by general theoretical arguments (Saleur and Sornette 1996).

(iii) **Search interval for t_c given by** $t_2 + 1 < t_c < t_2 + \eta||t_2 - t_1||$, where time is in units of days. $[t_1, t_2]$ is the time window in which the calibration is performed. One can think of t_2 as the 'present' time, in the sense that it is the latest time at which information is used to calibrate the model. The beginning t_1 of the fitting interval sets the time scale $t_2 - t_1$ of the analysis. The factor η is of the order of 1, often chosen about $1/3$ or $1/2$ to ensure that the remaining bubble lifetime is within an horizon of predictability estimated to scale proportionally to the width of the analysing window.

(iv) **'Damping' condition:** Within the RE bubble framework used by the JLS model, the crash hazard rate is found to be proportional to the expected return during the bubble, conditional on the fact that the bubble has not yet burst. Since the crash hazard rate is by definition a nonnegative quantity, this imposes that the expected return during the bubble should be nonnegative. This can be shown to impose that condition $D \geq 1$ where $D := \frac{|B|m}{\omega\sqrt{C_1^2+C_1^2}}$ (Graf v. Bothmer and Meister 2003). Intuitively, the amplitude of the log-periodic oscillations should be not too large compared with the acceleration of the price so that their combination ensures the nonnegativity of the expected return at all times during the bubble. Of course, the realized stochastic return can be negative. It is only its expectation that should be nonnegative.

(v) **Number of oscillations:** The number of oscillations (half-periods) of the log-periodic component is given by $O := \frac{\omega}{\pi}\ln\left(\frac{t_c - t_1}{t_c - t_2}\right)$. Huang *et al*. (2000) showed that a minimum number of oscillations is needed to distinguish a genuine log-periodic signal from one that could be generated by noise. In the present implementation, we qualify a fit only if $O \geq 2.5$.

(vi) **residuals $r \sim$ AR(1):** Lin *et al*. (2014) have emphasized the need for the residuals of the LPPLS calibration to be mean-reverting in order for the calibration of the log-price by the LPPLS model (3) to be consistent. Hence, we test for the mean-reverting (O-U) property of the residuals of the fit, using both the standard unit-root Augmented Dickey–Fuller and Phillips–Perron tests.

2.4. Expanded parameter space to endogenize t_1

Because the goal of the present article is to determine which of the beginning or the end of a bubble is best estimated, we propose to endogenize the search for the beginning of the bubble in the calibration of the parameters. For this, we define the beginning of the bubble as the 'best' beginning time t_1 of the interval $[t_1, t_2]$ in which the calibration is performed, 'best' in the sense of minimizing an appropriate scaled goodness of fit in combination with filtering conditions 1–6 presented on section 2.3. As we shall see, it is not possible to rely solely on the scaled goodness of fit measure because this metric is essentially degenerate as the number degrees of freedom is reduced. More specifically, as $t_1 \to t_2$ the metric tends to yield smaller and smaller values even when scaled due the reduced number of data points used for fitting the model. However, since plateaus are observed in certain values of t_1 our results can be trustworthy when analysing the cost function through a local perspective rather than a global one. This leads to an expanded nonlinear parameter set $\mathbf{\Phi} = \{m, \omega, t_c, t_1\}$. The L^2 cost function to minimize generalizes expression (A5) in appendix 1 to make explicit the beginning time t_1 of the time interval in the optimization problem. In order to make different windows $[t_1, t_2]$ comparable, we normalize the sum of squares of the residuals by the number $t_2 - t_1$ of points in the sum (Tsay 2010)

$$\chi^2(\mathbf{\Phi}) := F_2(m, \omega, t_c, t_1) = \frac{1}{t_2 - t_1} \sum_{i=t_1}^{t_2} r_i(\mathbf{\Phi})^2,$$
$$\text{with } r_i(\mathbf{\Phi}) = y(t)_i - flppl(\mathbf{\Phi}, t)_i, \qquad (4)$$

where $flppl(\mathbf{\Phi}, t)_i$ is defined by expression (A1) in appendix 1. The calibration of the parameters $\mathbf{\Phi}$ is performed by following the same procedure as explained in appendix 1, which is explicated in appendix 2.

2.5. Hessian matrix, its eigenvalues and eigenvectors quantifying rigidity vs. sloppiness

Since we are interested in the *relative parameter variations* and their corresponding impact upon χ^2, each parameter $[m, \omega, t_c, t_1] \in \mathbf{\Phi}$ was standardized using

$$\tilde{\Phi}_i = \frac{\Phi_i - \langle \Phi_i \rangle}{\sigma(\Phi_i)}, \qquad (5)$$

where $\langle \Phi_i \rangle$ and $\sigma(\Phi_i)$ denotes, respectively, the median and the standard deviation of parameter i within its respective theoretical bound (see conditions 1–3 in section 2.3). This transformation ensures that the mean of $\tilde{\Phi}_i$ is 0 and its standard deviation is equal to 1 for all four nonlinear parameters. This allows us to compare their sloppiness (Brown and Sethna 2003) based on a study of the Hessian matrix given by equation (B10) in appendix 2.

Once the optimal parameter set $\mathbf{\Phi}^*$ is obtained and after standardization, we computed the Jacobian $J(\mathbf{\Phi}^*)$ defined by (B5) using equation (B10) in appendix 2. For small residuals $\boldsymbol{r}$, the Hessian matrix about the best-fit is then approximated by equation (B8) using $\boldsymbol{J}^\intercal \boldsymbol{J}$. Recall that the Hessian matrix provides a quantification of the shape of the cost function in parameter space. The spectrum of eigenvalues $\{\lambda_i\}$ and their associated eigenvectors $\{\vec{v}_i\}$ of the Hessian matrix embody the information on the directions in parameter space that are best determined. Large eigenvalues correspond to rigid parameters (or combination of parameters), i.e. for which a small variation entails a relatively large change of the cost function. In contrast, small eigenvalues identify the 'sloppy' parameters (or combination of parameters) that are poorly constrained, so that a rather large variation of their value does not change much the cost function. Geometrically, one can picture the cost function as made of wide valleys with elongated flat profiles along the eigenvectors with small eigenvalues, and of sharp narrow valleys along the eigenvectors with large eigenvalues. If, as we find below, a given eigenvector is dominated by one of the parameters, its corresponding eigenvalue determines the rigidity vs. sloppiness of that parameter (rigid if the eigenvalue is relatively large and sloppy if small).

In practice, fits whose spread between the largest and the smallest eigenvalue surpasses roughly three orders of magnitude are considered *sloppy* (Machta *et al*. 2013). Generally, this results from a near degenerate Hessian matrix (see equation (B6)), where changes in a given parameter do not lead to an increase in the cost function since this change can be compensated by that of another parameter along the sloppy direction. It is important to keep in mind, however, that even though large parameter uncertainty does in general exist, the macroscopic behaviour of the system is not necessarily compromised (Bak *et al*. 1988, Transtrum and Sethna 2012), given that predictions rely on rigid directions of the model.

2.6. Construction of synthetic LPPLS bubbles

To gain insight about the parameter structure of the extended LPPLS model and thus establish a solid background to our empirical analysis, we generate synthetic price time series. The synthetic price time series (a realization is depicted in figure 1(a)) are obtained by using formula (3) with parameters given by the best LPPLS fit within the window $w \in [t_1 =$ January 1981: $t_2 =$ August 1987] of the bubble that ended with the Black Monday 19 October 1987 crash. These parameters are $m = 0.44$, $\omega = 6.5$, $C_1 = -0.0001$, $C_2 = 0.0005$, $A = 1.8259$, $B = -0.0094$, $t_c = 1194$. To the deterministic component describing the expected log-price given by expression (3) and denoted by $flppls(\boldsymbol{\phi}, t)$ (as in appendix 1, see expression (A1)), we add a stochastic element according to

$$\ln[P(t)] = flppls(\phi, t)\left(\frac{1 + \varepsilon(t)\,\sigma}{\max(lppls(t))}\right), \qquad (6)$$

where $t = [1, \ldots, N = 1100]$. This corresponds to multiplicative (or proportional) noise term with $\varepsilon \sim \mathcal{N}(\mu, \sigma^2)$ and $\sigma = 0.1$, $\mu = 0$. The black stochastic line in figure 1(a) represent $\ln[P(t)]$ given by (6).

For each synthetic bubble price time series, we calibrated it with equation (3) by minimizing expression (4) in windows $[t_1, t_2]$, scanning t_2 from 1 January 1981 to 12 August 1987, with t_1 varying from $t_1 =$ January 1981 up to 60 business days before t_2, i.e. up to $t_{1,\max} = t_2 - 60$ for each fixed t_2. Then, the Hessian matrix was approximated about the best-fit parameters for each t_1 and its corresponding eigenvalues were calculated.

2.7. Sloppiness and rigidity of t_c vs. t_1 using synthetic price time series

We now extend the initial sloppy-rigid analysis performed in the LPPLS framework by Bree *et al*. (2013), in order to test which one of the two parameters, beginning t_1 or the forecasted end $\widehat{t_c}$ of a bubble, is the most sloppy, i.e. has the largest uncertainty.

For illustration of the typical situation found in these synthetic tests (to be extended below), we perform the calibration of synthetic noisy price time series in the full window shown in figure 1 corresponding to [$t_1 =$ January 1981 to $t_2 =$ August 1987] (represented as $[Date = 1 : Date = 1100]$). For a given realization, we calculate the Hessian matrix and the corresponding eigenvalues and eigenvectors. We consider both the case of a fixed t_1 with cost function (A5) (bottom rows of table 1) and of the extended cost function (4) endogenizing t_1 as a parameter to be determined (top rows of table 1). The entries of the two Hessian matrices are given in the columns on the left of the table and their eigenvalues in the central column λ (table 2).

Note first that the smallest eigenvalue is of the order 10^{-8} times the largest eigenvalue, exemplifying the sloppy nature of the calibration. In the right columns of the table, the components of the corresponding eigenvectors show that the largest eigenvalue is mainly determined by parameter m, the second largest one is mainly controlled by parameter ω and the smallest

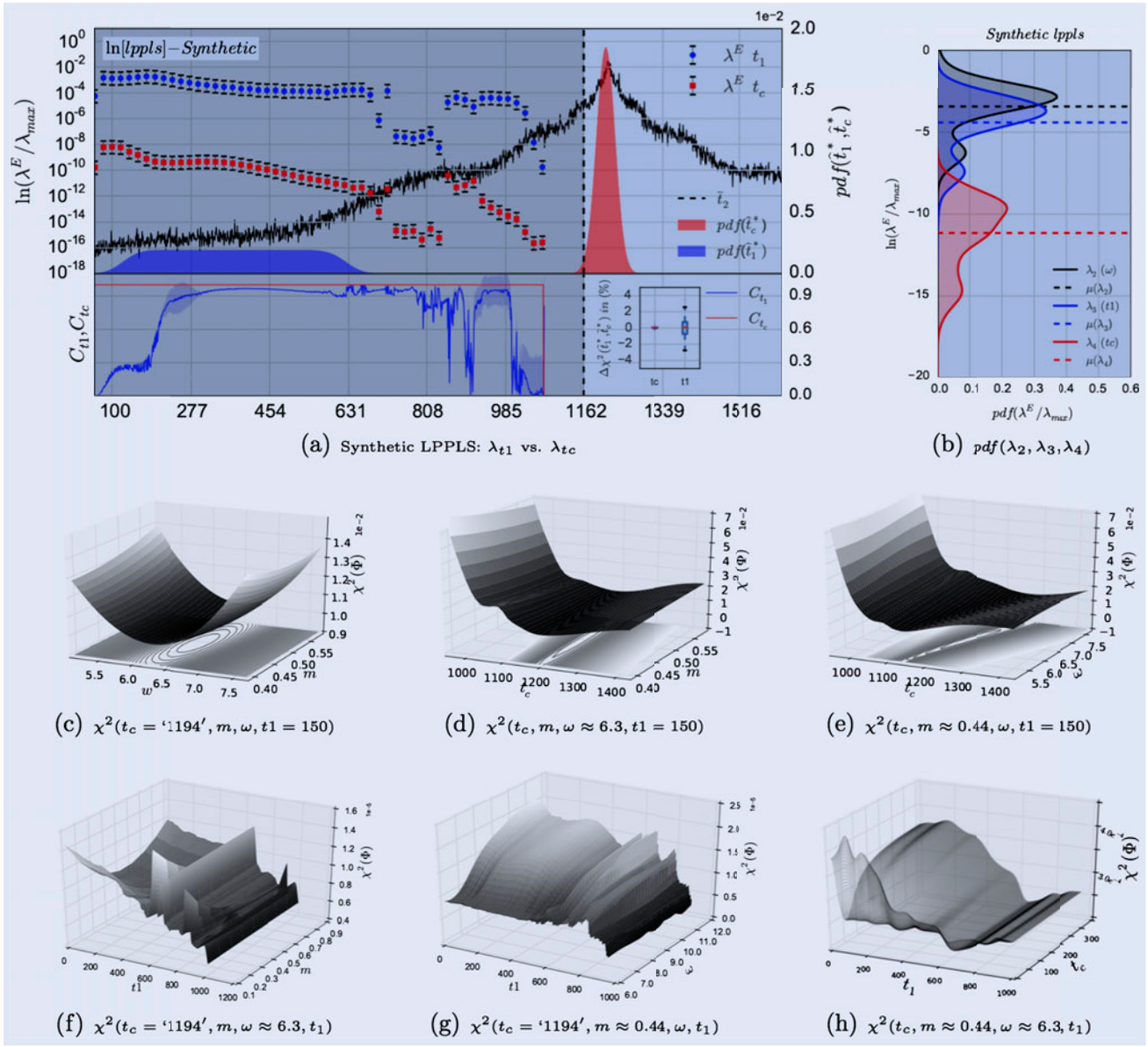

Figure 1. Quantification of the relative sloppiness of t_c and t_1 in synthetic data: (panel (a)): a synthetic noisy LPPLS price time series generated as described in the main text is shown with the black continuous line. Here, the *x-axis* denote values of the beginning t_1 of the window in which the calibration is performed at a fixed $\bar{t}_2$. The blue circles and red squares show the normalized eigenvalues (λ) of the Hessian matrix $H(\Phi^*)$ estimated at the best-fit, which correspond mainly to the directions t_1 and t_c in parameter space, (see figure 5 for precise quantification). Errors bars for each parameter represent $\lambda_i^E \pm \sigma(\lambda_i^E)$ over 100 realizations (corresponding to 100 generations of the noise). The relative contribution (see equation (7)) of t_1 and t_c at eigenvalues λ_3 and λ_4 is depicted using coloured lines within the grey-shaded area. Coloured pdf's denote qualified values of t_1 and t_c at $\bar{t}_2$. The inset box-plot shows the normalized cost change in % terms when t_1 (respectively, t_c) are perturbed over the ensemble of $\widehat{t_1^*}$ (respectively, $\widehat{t_c^*}$). Panel (b) shows the distributions over the ensemble of t_1 values of the Hessian eigenvalues for the aggregated LPPLS fits performed in the synthetic data. From top to bottom, the *y-axis* display the hierarchy (rigid to sloppy) of parameters that govern the model output. Panels (c)–(h): cross sections of the cost function $\chi^2(\Phi)$ at the best-fit window ($w \equiv ||t1^* : t2^*||$, i.e. for the window starting at the fitted t_1 for the fixed $t_2 = 150$) in the planes (m, ω), (t_c, ω), (t_c, m), (t_1, m), (t_c, ω) and (t_1, t_c), respectively.

eigenvalue is always mainly associated with parameter t_c, confirming that the end of the bubble is very difficult to determine as the cost function is essentially degenerate in the direction of t_c in parameter space.

Interestingly, for the extended cost function, one can observe that the eigenvalue dominated by parameter t_1, while being smaller than the two others associated with m and ω, is approximately 4000 times larger that the eigenvalue describing the sloppiness of t_c. This is a first illustration that t_1 is much more rigidly determined (or depending on taste much less sloppy) than t_c. Indeed, using a geometrical intuitive interpretation, contour lines of the cost function form approximate ellipses whose axis lengths are inversely proportional to the square root of their corresponding eigenvalue λ (axis length $\simeq 1/\lambda^{\frac{1}{2}}$). Thus a factor 4000 translates into a size of the axis along t_c about 60 times larger than the axis along t_1. In other words, in this illustration, the uncertainty on t_1 is about 60 times smaller than on t_c.

Does this result hold for other time windows and in particular far from the end of the bubble? To investigate this question, we perform the same exercise of calibrating the LPPLS formula in windows $[t_1, t_2]$, varying t_1 from $Date = 1$ (about four

Table 1. Hessian matrix (left columns), eigenvalues λ (middle column) and corresponding eigenvectors $\vec{v}$ (right columns), for the best LPPLS fits of the synthetic price time series generated as explained in section 2.7 using $\chi^2(\phi)$ and $\chi^2(\Phi)$ in the full window shown in figure 1(a) corresponding to [t_1 = January 1981 to t_2 = August 1987] (represented as [$Date = 1 : Date = 1100$]). The top rows correspond to the extended cost function (4) endogenizing t_1 as a parameter to be determined. The bottom rows correspond to the case of a fixed t_1 with cost function (A5).

	lppls synthetic								
	Hessian, H(Φ^*)					Eigenvectors, $\vec{v}$			
	m	ω	t_c	t_1	λ/λ_{max}	m	ω	t_c	t_1
m	9.20e−1		8		1.00e0	**−9.99e−1**	−4.40e−2	−9.73e−5	−4.37e−4
w	4.05e−2	3.70e−03			2.07e−3	−4.40e−02	**9.98e−1**	−2.05e−3	−9.22e−3
t_c	8.98e−5	2.02e−08	5.12e−07		1.06e−4	8.43e−4	−9.19e−3	5.27e−4	**−9.99e−1**
t_1	4.04e−4	1.07e−06	2.40e−08	9.87e−05	5.37e−7	1.88e−4	−2.05e−3	**−9.99e−1**	−5.08e−4
	Hessian, H(ϕ^*)					Eigenvectors, $\vec{v}$			
	m	ω	t_c		λ	m	ω	t_c	
m	5.91e−2				1.00e0	**9.98e−1**	3.59e−2	1.69e−3	
ω	−1.96e−3	4.71e−3			7.84e−2	3.60e−2	**9.99e−1**	1.54e−2	
t_c	9.78e−5	−7.53e−5	1.41e−6		2.35e−6	1.13e−3	1.55e−2	**9.99e−1**	

Table 2. Hessian matrix, eigenvalues and corresponding eigenvectors for the best LPPLS fits using equation (4) of the financial bubbles described in section 3.1 in the time windows [$t_1^* : t_2$] given in the table for each bubble. The numbers in boldface indicate the parameters that contribute the most to their eigenvectors.

S&P 500 (BM)									
$t_1^* \approx$ March 1984, $t^2 \approx$ August 1987									
	Hessian, H(Φ^*)					Eigenvectors, $\vec{v}$			
	m	ω	t_c	t_1	λ/λ_{max}	m	ω	t_c	t_1
m	9.20e−1				1.00e0	**−9.99e−1**	−1.90e−2	−3.81e−4	−9.81e−3
ω	1.68e−2	3.70e−2			4.05e−2	−2.02e−2	**9.90e−1**	2.07e−3	1.36e−1
t_c	3.45e−4	8.20e−7	9.87e−4		4.90e−3	7.07e−3	1.35e−1	−1.64e−1	**−9.77e−1**
t_1	8.90e−3	4.63e−3	5.96e−4	5.12e−3	9.65e−4	−8.34e−4	−2.05e−2	**−9.86e−1**	1.63e−1
S&P 500 (SP)									
$t_1^* \approx$ December 2003, $t^2 \approx$ July 2007									
	Hessian, H(Φ^*)					Eigenvectors, $\vec{v}$			
	m	ω	t_c	t_1	λ/λ_{max}	m	ω	t_c	t_1
m	9.20e−1				1.00e0	**−9.99e−1**	−2.12e−2	−6.61e−4	−1.21e−3
ω	1.320e−2	3.00e−1			3.26e−1	−2.13e−2	**9.99e−1**	−8.57e−6	3.18e−2
t_c	6.09e−4	7.85e−6	1.87e−5		2.31e−3	−5.59e−4	−3.18e−2	3.78e−2	**9.98e−1**
t_1	9.12e−4	9.50e−3	8.07e−5	2.43e−3	1.65e−5	−6.41e−4	1.20e−3	**9.99e−1**	−3.78e−2
SSEC									
$t_1^* \approx$ February 2005, $t^2 \approx$ October 2007									
	Hessian, H(Φ^*)					Eigenvectors, $\vec{v}$			
	m	ω	t_c	t_1	λ/λ_{max}	m	ω	t_c	t_1
m	5.22e−1				1.00e0	**−9.99e−1**	−1.26e−2	−3.75e−5	−1.74e−3
ω	6.32e−3	2.28e−2			4.35e−2	−1.26e−2	**9.99e−1**	3.01e−4	2.33e−2
t_c	1.95e−5	7.03e−6	9.81e−5		3.67e−3	1.44e−3	2.34e−2	−9.82e−4	**−9.99e−1**
t_1	9.02e−4	4.98e−4	1.98e−6	1.93e−3	1.87e−4	3.22e−5	2.78e−04	**−9.99e−1**	9.89e−4
IBovespa									
$t_1^* \approx$ June 2003, $t^2 \approx$ January 2004									
	Hessian, H(Φ^*)					Eigenvectors, $\vec{v}$			
	m	ω	t_c	t_1	λ/λ_{max}	m	ω	t_c	t_1
m	2.60e−1				1.00e0	**−9.99e−1**	−4.00e−3	−3.84e−6	−3.86e−5
ω	1.01e−3	2.03e−02			3.95e−2	−4.00e−3	**9.99e−1**	2.30e−7	2.12e−4
t_c	2.09e−6	6.16e−9	9.82e−6		3.77e−3	3.77e−5	2.12e−4	−1.02e−3	**−9.99e−1**
t_1	1.12e−05	2.02e−6	1.10e−6	9.82e−4	3.77e−5	3.80e−6	2.67e−8	**−9.99e−1**	1.02e−3

years before the crash) to $Date = 1040$ days (close to the crash). The blue circles and red squares in figure 1 display the obtained normalized eigenvalues λ_3 and λ_4 in logarithm scale, associated, respectively, to t_1 and t_c. By 'normalized', we mean that each eigenvalue obtained for a given calibration is divided by the largest one (i.e. that associated mainly with m). By repeating this process 100 times, confidence bounds for the eigenvalues for each t_1 can be determined and are depicted by the error bars. Figure 1 confirms that t_1 is always more rigid that t_c by far at all times t_2. It is particularly noteworthy that the situation for t_c does not improve in absolute terms or relative to t_1 even when getting closer and closer to the true end of the bubble: while the determination of the beginning t_1 of the bubble can be reasonably estimated, that of the end t_c remains much more elusive. One can also observe a rather stable behaviour of these two eigenvalues when t_1 spans 1 to 600 days. Interestingly, the vast majority of fits performed during this time window correctly qualify the underlying time series as being in a bubble regime.

For Date $= t_1 > 600$, one can observe a fast drop of the eigenvalues associated with t_1 and t_c, which can be explained by the average negative curvature of the log-price associated with the first large log-periodic oscillation. This negative curvature confounds the information on the existence of the supposed super-exponential bubble and thus on the determination of both its beginning (t_1) and its end (t_c). When the average curvature of the log-price becomes positive again, one can observe a jump of the two eigenvalues upward, back to almost the same level as before the first jump down. This is followed by a further decrease in the eigenvalues as t_1 approaches too close to the true t_c.

The lower part of panel (a) of figure 1 checks that the two smallest eigenvalues λ_3 and λ_4 are indeed mostly representing, respectively, the directions along t_1 and t_c of the cost function. To quantify that this is the case, let us denote $\vec{v}(t_{1,\lambda_3})$ the component on t_1 of the third vector associated with the third largest eigenvalue λ_3. Similarly, let $\vec{v}(t_{c,\lambda_4})$ be the component on t_c of the fourth vector associated with the smallest eigenvalue λ_4. Analogously, $\vec{v}(\Phi_j, \lambda_i)$ is the component on parameter Φ_j of the eigenvector associated with the eigenvalue λ_i. Let us introduce the weights

$$C_{t_1,\lambda_3} = \frac{|\vec{v}\,(t_{1,\lambda_3})|}{\sum_{j=1}^{4}\sqrt{\vec{v}\,(\Phi_j,\lambda_3)^2}},$$
$$C_{t_c,\lambda_4} = \frac{|\vec{v}\,(t_{c,\lambda_4})|}{\sum_{j=1}^{4}\sqrt{\vec{v}\,(\Phi_j,\lambda_4)^2}}. \quad (7)$$

These weights C_{t_1,λ_3} and C_{t_c,λ_4} are shown in the lower part of panel (a) of figure 1 and confirm that the relative contributions of parameter t_1 (resp. t_c) in the eigenvector along λ_3 (resp. λ_4) is never smaller than $\approx 90\%$ (respec. 99%).

The distributions of the normalized eigenvalues λ_2/λ_1, λ_3/λ_1 and λ_4/λ_1 over the ensemble of t_1 values for a fixed t_2 and a single log-price realization are depicted in figure 1(b). The dashed lines show the mean values of the three distributions. This confirms that t_1 is much more rigid than t_c across all windows and that the hierarchy from rigid to sloppy is from m, ω, t_1 to t_c.

For the fixed Date $t_2 = 150$, figure 1(c)–(h) show cross sections of the cost function for parameters m, ω, t_1 and t_c. The shape of the cost function exhibits the valley patterns whose relative extensions in different directions are quantified by the eigenvalues, as discussed above. Figure 1(c) and (d) shows that, for parameters m vs. ω and m vs. t_c, the elliptic contour lines close to the cost function minimum are aligned approximately along the parameter axes. In contrast, for the parameter space of t_c vs. ω, the largest eigen-direction is along the diagonal direction. This feature expresses the fact that parameters ω and t_c are strongly correlated in the calibration process. In practice, this implies the existence of several values of t_c that are consistent with a low cost value, given that parameter ω (see figure 1(e)) can be tuned to take this variation into account. Thus, this interdependency should be considered properly when constructing confidence intervals for ω and t_c, as correctly pointed out by Bree *et al.* (2013).

For robustness, a sensitive analysis was performed around the best solutions of $\widehat{t_1^*}$ and $\widehat{t_c^*}$. By taking into account the sample size, the box-plot shown in figure 1(a) gives the corresponding χ^2 variation when each $t_1 \in \widehat{t_1^*}$ and $t_c \in \widehat{t_c^*}$ are used as input parameters in equation 4. Results confirm that changes in t_1 leads to cost variations ranging from -4% to 4% while changes in $\widehat{t_c^*}$ yields a negligible change. This is due to the compensation provided by the correlation between ω and the critical time parameter (see figure 1(e)) previously mentioned.

Finally, the caoloured *pdf's* in figure 1(a) were constructed over the qualified fits (according to the filtering criteria of section 2.3) of the ensemble of noise realizations for a fixed $\bar{t}_2$. The fact that the $pdf(\widehat{t_1^*})$ is wider than $pdf(\widehat{t_c^*})$ is not contradicting our key result that t_1 is much better estimated than t_c *for a specific realization*. In a real-life situation, one can only analyse one single realization given by history. In contrast, the coloured $pdf's$ in figure 1(a) provide artefactual information, i.e. on an ensemble of statistically equivalent price trajectories differentiated only by the different realizations of the noise process. The fact that the $pdf(\widehat{t_1^*})$ is wider than $pdf(\widehat{t_c^*})$ thus inform us that there is more variability of t_1 than t_c from one realization to another one. This results from the structure of log-periodicity, with slow oscillations at early times and fast oscillations close to t_c.

3. Empirical tests

3.1. Data: eight historical bubbles

In this section, we perform the same procedure as described in the previous section on real bubble events. Scanning a time interval extending from several years before until the burst of each bubble, we first determine the time $\bar{t}_2$ at which the price reached its maximum before the crash starts to develop. We fix this time as the end of our time window of analysis. Obviously, this procedure is not correct for forecasts as it uses future information (the fact that $\bar{t}_2$ was the maximum before the crash) but is useful to reduce the number of degrees of freedom for our purposes. Further down, we drop this assumption and incorporate random $t_2's$ into the analysis (see 3.3). For this fixed $\bar{t}_2$, our fitting windows scan t_1 using daily observations ranging from some $t_{1,i=1}$ until $t_{1,\bar{t}_2-60}$, where the unit of time is one day, which are used as input for the t_1 parameter during the calibration process (4).

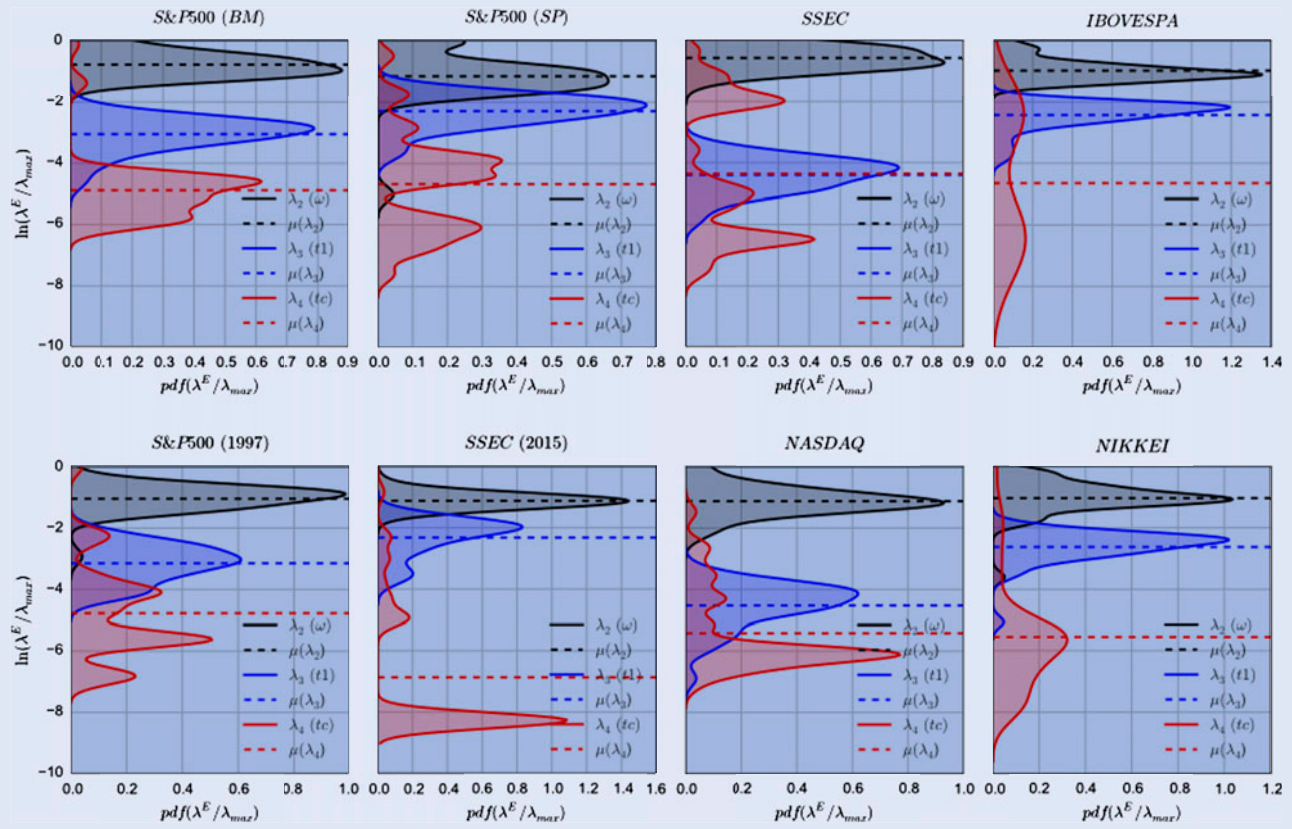

Figure 2. Probability density functions (pdf) of the normalized eigenvalues λ_2/λ_1, λ_3/λ_1 and λ_4/λ_1 over the ensemble of windows obtained by scanning t_1 for the eight empirical bubbles described in section 3.1. The horizontal dashed lines indicate the mean values of the distributions. The colors of the pdf's encode the parameter that dominates its corresponding eigenvalue: green for m ($\lambda/\lambda_{\max} = 0 = 1.00e0$), grey for ω, blue for t_1 and red for t_c.

We have chosen a representative set of eight well-known bubbles, augmented by the synthetic bubbles given by (6) for comparison.

- **Shanghai Stock Exchange Composite Index bubble ending in October 2007 (SSEC):**
  This bubble has been documented and studied by Jiang *et al.* (2010). For $\bar{t}_2 = 10$ October 2007, our fitting windows scan t_1 using daily observations ranging from $t_{1,i=1} = 1$ January 2005 until $t_{1,\bar{t}_2-60} = 10$ August 2007. Converting from calendar time to time counted in unit of days, we have $t_{1,i=1} = 1$ and $\bar{t}_2 = 676$. Thus, there are 616 different possible windows for the fixed end time $\bar{t}_2 = 676$, the different windows corresponding to the different $t_{1,1} = 1$, $t_{1,2} = 2$, ..., $t_{1,\bar{t}_2-60} = 616$, which are used as input for the t_1 parameter during the calibration process (4). Note that the smallest (resp. largest) window has a duration of 60 (resp. 676) days.
- **S&P500 Index bubble ending in October 2007 (SP):**
  This bubble has been documented and studied in Sornette and Woodard (2010), Sornette and Cauwels (2014), Sornette and Cauwels (2015). The same procedure as described for the previous bubble was applied to the $S\&P500$. With the choice $\bar{t}_2 = 15$ July 2007, our fitting windows scan t_1 using daily observations ranging from $t_{1,i=1} = 1$ January 2002 to $t_{1,\bar{t}_2-60} = 1$ May 2007. This yields a total of $N = 1332$ different possible values of t_1 over which to perform the calibration process (4).
- **S&P500 Index bubble ending on Black Monday, 19 October1987 (BM):**
  This bubble has been documented and studied by Sornette *et al.* (1995). Choosing $\bar{t}_2 = 15$ August 1987, our fitting windows scan t_1 using daily observations ranging from $t_{1,i=1} = 1$ January 1981 until $t_{1,\bar{t}_2-60} = 12$ June
  1987. This yields a total of $N = 1674$ different possible values of t_1 over which to perform the calibration process (4).
- **Bovespa Index bubble ending in December 2003:**
  Choosing $\bar{t}_2 = 15$ December 2003, our fitting windows scan t_1 using daily observations ranging from $t_{1,i=1} = 1998/06/22$ until $t_{1,\bar{t}_2-60} = 14$ October 2003. This yields a total of $N = 1940$ different possible values of t_1 over which to perform the calibration process (4).
- **S&P500 Index short-term bubble ending in February 1997:**
  With the choice $\bar{t}_2 = 13$ February 1997, our fitting windows scan t_1 using daily observations ranging from $t_{1,i=1} = 24$ August 1991 to $t_{1,\bar{t}_2-60} = 1$ May 1997. This yields a total of $N = 1940$ different possible values of t_1 over which to perform the calibration process (4).
- **Shanghai Stock Exchange Composite Index bubble ending in June 2015:**
  A detailed real-time diagnosis and post-mortem analysis of the Shanghai 2015 bubble and subsequent crash can be found in Sornette *et al.* (2015). With $\bar{t}_2 = 10$ June

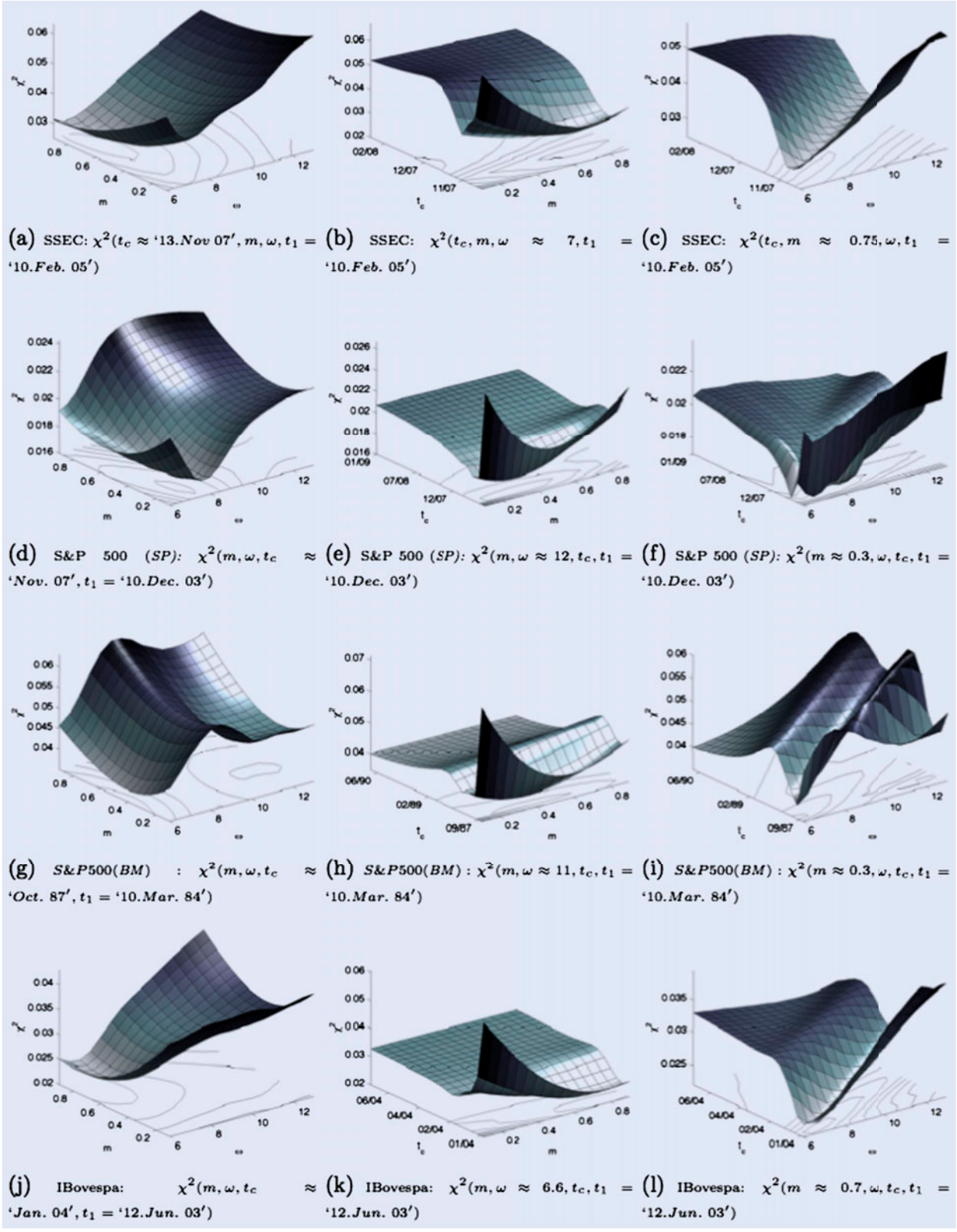

Figure 3. Cross sections of the cost function $\chi^2(\Phi)$ for the eight studied empirical bubbles described in section 3.1 along the three different pairs of structural parameters (m, ω), (t_c, m) and (t_c, ω). Small (resp. large) values for the cost function correspond to lighter (resp. darker) colours and depict parameter domains giving better fits.

2015, our fitting window scan t_1 using daily observations ranging from $t_{1,i=1} =$ 18 December 2009 until $t_{1,\bar{t}_2-60} =$ 11 April 2015 thus yielding a total of $N =$ 1940 different possible values of t_1 over which to perform the calibration process (4).

- **NASDAQ (dot-com bubble) ending in February 2000:** Searching for the beginning of this bubble at $\bar{t}_2 =$ 20 February 2000, we scan t_1 using daily observations ranging from $t_{1,i=1} =$ 1 September 1994 until $t_{1,\bar{t}_2-60} =$ 24 December 1999 thus yielding a total of $N =$ 1940

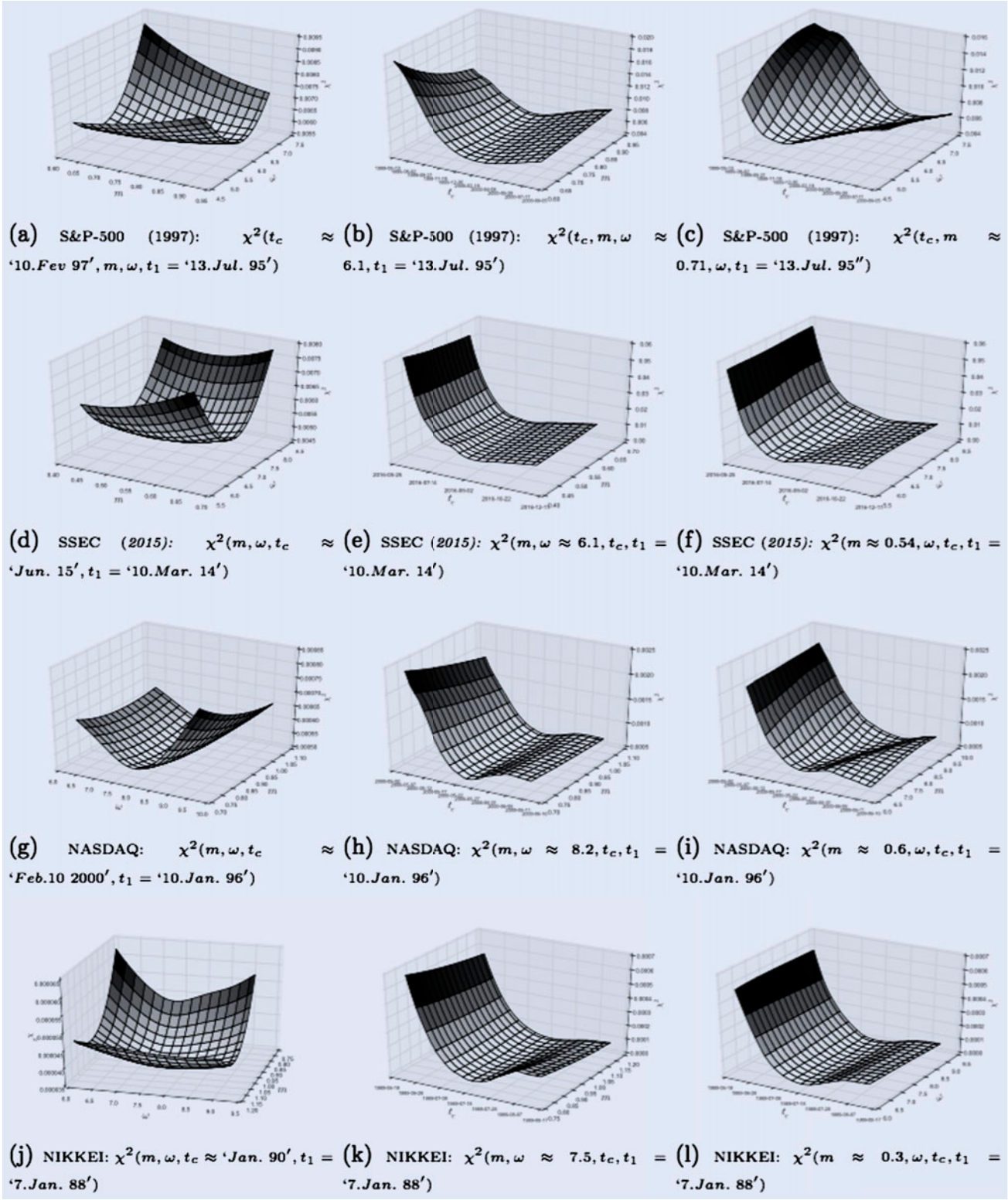

Figure 4. Cross sections of the cost function $\chi^2(\Phi)$ for the *S&P*500, SSEC, NASDAQ and NIKKEI Indexes empirical bubbles described in section 3.1 along the three different pairs of structural parameters (m, ω), (t_c, m) and (t_c, ω). Small (resp. large) values for the cost function correspond to lighter (resp. darker) colours and depict parameter domains giving better fits.

different possible values over which to perform the calibration process (4).

- **NIKKEI Index bubble ending in January 1999:** With the choice $\bar{t}_2 =$ 10 December 1989, our fitting windows scan t_1 using daily observations ranging from $t_{1,i=1} =$ 19 June 1984 to $t_{1,\bar{t}_2-60} =$ 11 October 1989. This yields a total of $N = 1940$ different possible values of t_1 over which to perform the calibration process (4).

For each of these eight empirical time series, the corresponding residuals $r(t)$'s defined in (4) are obtained for each window $[t_1, \bar{t}_2]$ and the set of their probability density functions (pdf) obtained when scanning t_1 are shown in figure 9 of the Supplementary Materials. Except from moments where

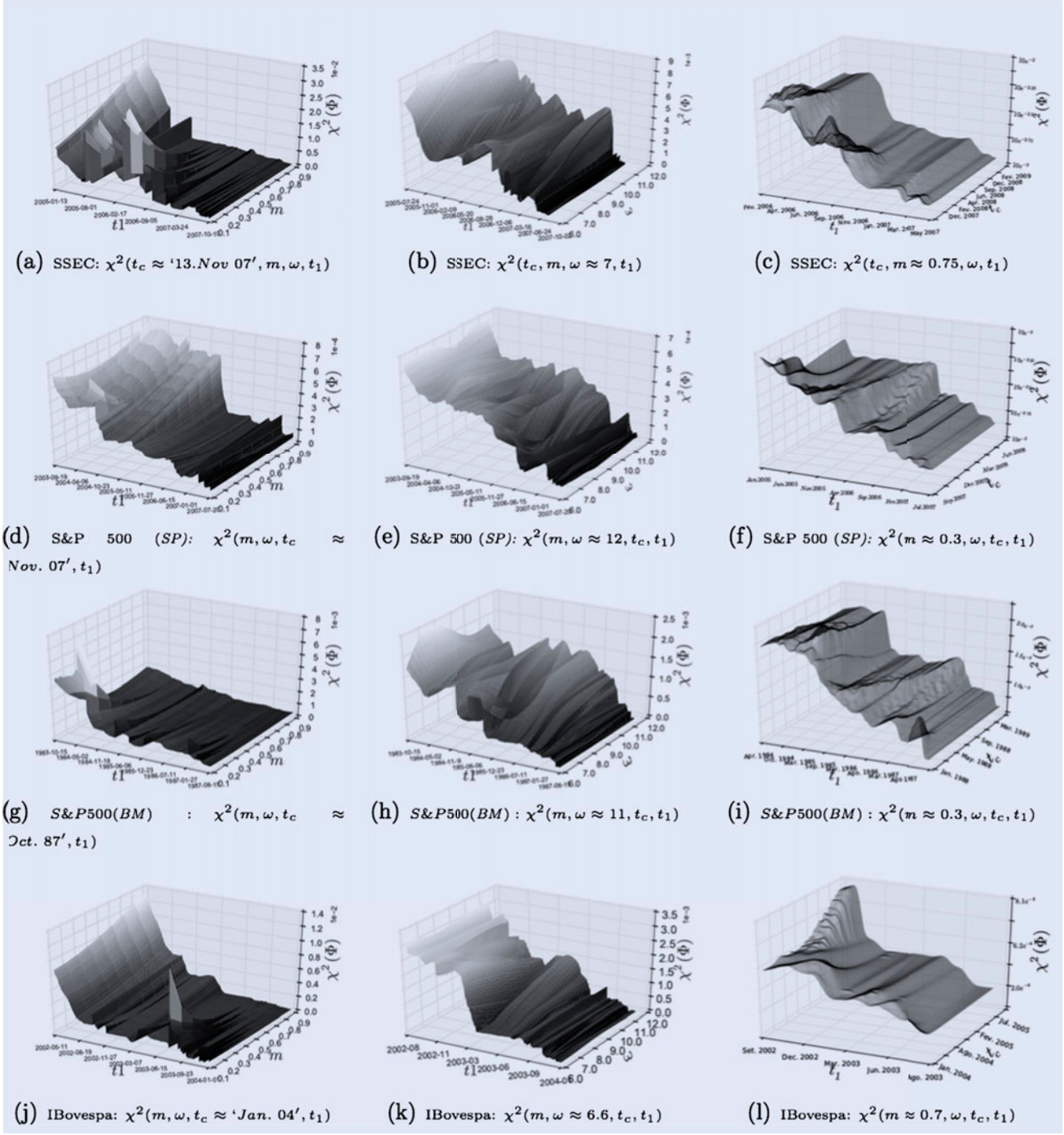

Figure 5. Cross sections of the cost function $\chi^2(\Phi)$ for the eight studied empirical bubbles described in section 3.1 along the three different pairs of parameters (t_1, m), (t_1, ω) and (t_1, t_c), outlining the dependence on the parameter t_1 representing the beginning of the bubble. Small (resp. large) values for the cost function correspond to lighter (resp. darker) colours and depict parameter domains giving better fits.

fits are not qualified, the residuals are well behaved and are approximately normally distributed.

3.2. *Analysis of the cost function* $\chi^2(\Phi)$ *and its Hessian*

For the eight empirical bubbles, figure 2 presents the pdf's of the normalized eigenvalues λ_2/λ_1, λ_3/λ_1 and λ_4/λ_1 of the Hessian matrix $H|^*_{(\Phi)}$, over the ensemble of t_1 values scanned in the analysis. As in table 1 obtained for a synthetic bubble, we find almost systematically that the largest eigenvalue is dominated by parameter m. The colours of the pdf's encode the parameter that dominates its corresponding eigenvalue: green for m, grey for ω, blue for t_1 and red for t_c. One can observe that the normalized λ_3 (blue pdf) associated predominantly with t_1 are systematically much larger than the values of the normalized λ_4 (red pdf) associated predominantly with t_c. This confirms for these eight empirical bubbles the conclusion obtained in the synthetic tests. Moreover, we find that more than 80% of the windows give a normalized $\lambda_2 > 10^{-3}$, allowing us to conclude that ω (and a fortiori m) is a relatively rigid parameter (figure 3).

Overall, the eigenvalues $\lambda_i^E \equiv \lambda_i$, for $i = [m, \omega, t_1, t_c]$ exhibit a mixture of jumps intercalated with intervals of stable downward trends as the window length shrinks and t_1 approaches t_2 (see figure 10 of the Supplementary Materials.).

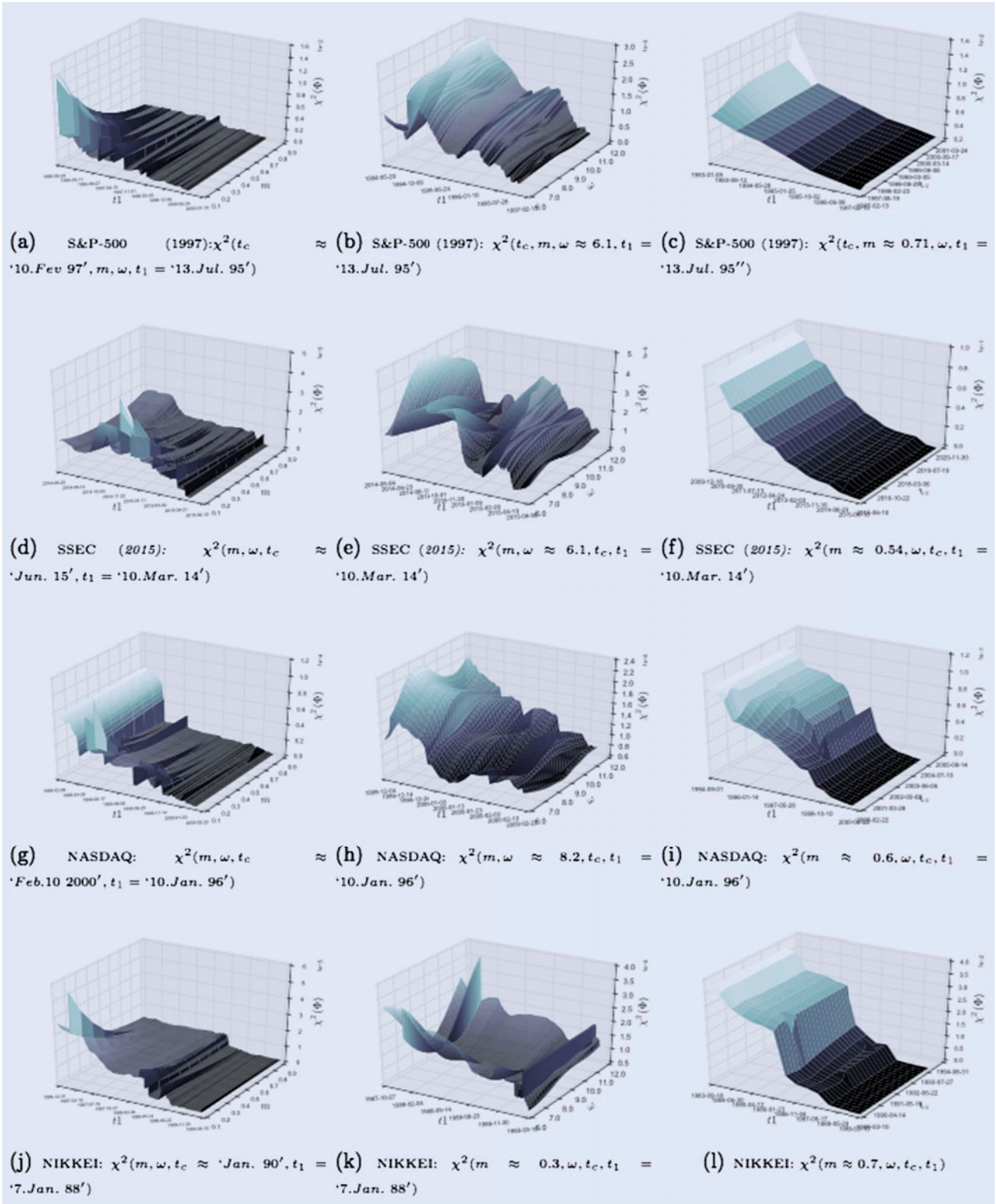

Figure 6. Cross sections of the cost function $\chi^2(\Phi)$ for the eight studied empirical bubbles described in section 3.1 along the three different pairs of parameters (t_1, m), (t_1, ω) and (t_1, t_c), outlining the dependence on the parameter t_1 representing the beginning of the bubble. Small (resp. large) values for the cost function correspond to lighter (resp. darker) colours and depict parameter domains giving better fits.

When using the original cost function (A5), the same pattern for the contribution of the parameters to the eigenvectors is observed as well as the same behaviour of the eigenvalues as a function of t_1 (see figure 11 in the Supplementary Materials). The overall sloppiness does not change substantially when using the extended cost function F_2 (expression (4)) instead of F_1 (see definition (A6)).

Figure 4 displays three two-dimensional cross sections of the cost function $\chi^2(\mathbf{\Phi}^*)$ for the eight empirical bubbles along the three different pairs of structural parameters (m, ω), (t_c, m) and (t_c, ω). The corresponding values of the Hessian matrix, eigenvectors and eigenvalues are summarized in table 3. Under the same conditions, table 4 gives the values of the Hessian matrix, of the eigenvalues λ and associated eigenvectors $\vec{v}$ us-

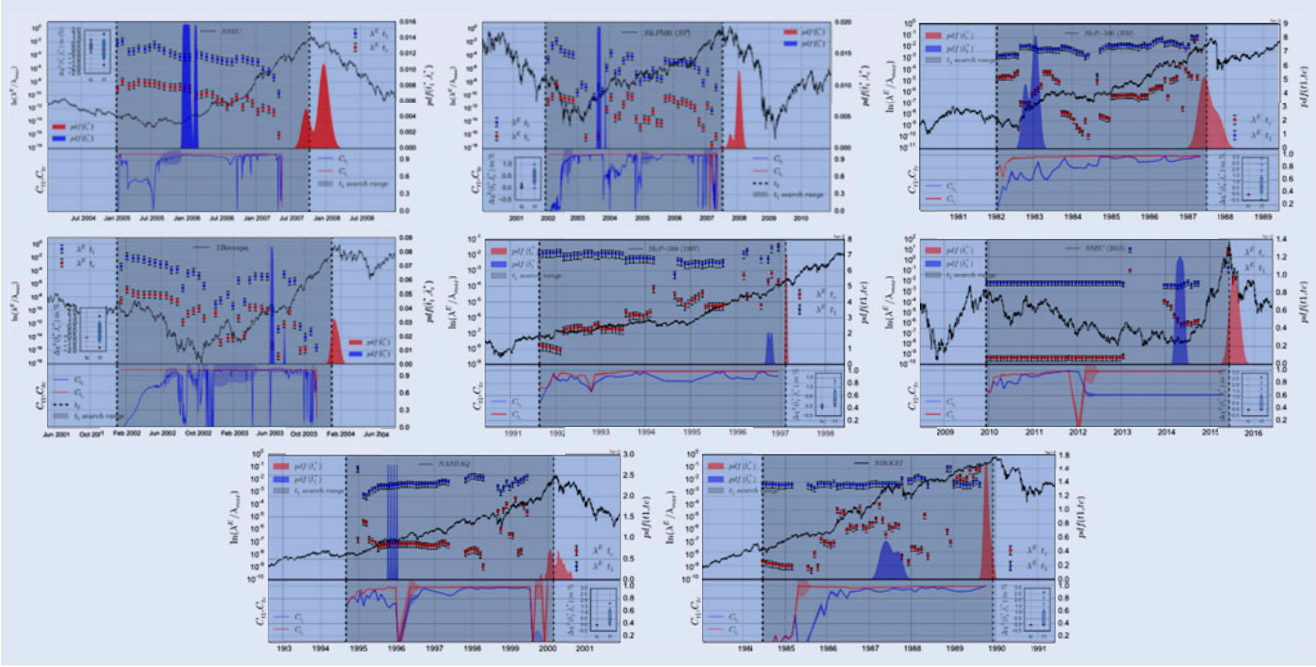

Figure 7. Quantification of the relative sloppiness of t_c and t_1 for the eight empirical bubbles described in section 3.1. The logarithm of their price as a function of time is shown by the black continuous line in each panel. The blue circles and red squares show the normalized eigenvalues λ_3^E and λ_4^E of the Hessian matrix $H(\Phi^*)$ estimated for the best-fit, respectively, mainly associated with t_1 and t_c, as a function of t_1 for a fixed t_2 indicated by the black vertical dashed line. The errors bars represent $\pm$ one-sigma interval around the mean values, obtained over 100 estimations. The relative contribution defined by expression (7) of t_1 to the eigenvalue λ_3 and of t_c to λ_4 are shown using vertical coloured lines inside the grey-shaded area. The box-plots in the inset show the normalized cost change in percent when t_1 (respectively, t_c) are sampled over the ensemble of calibrated $\widehat{t_1^*}$ (respectively, $\widehat{t_c^*}$).

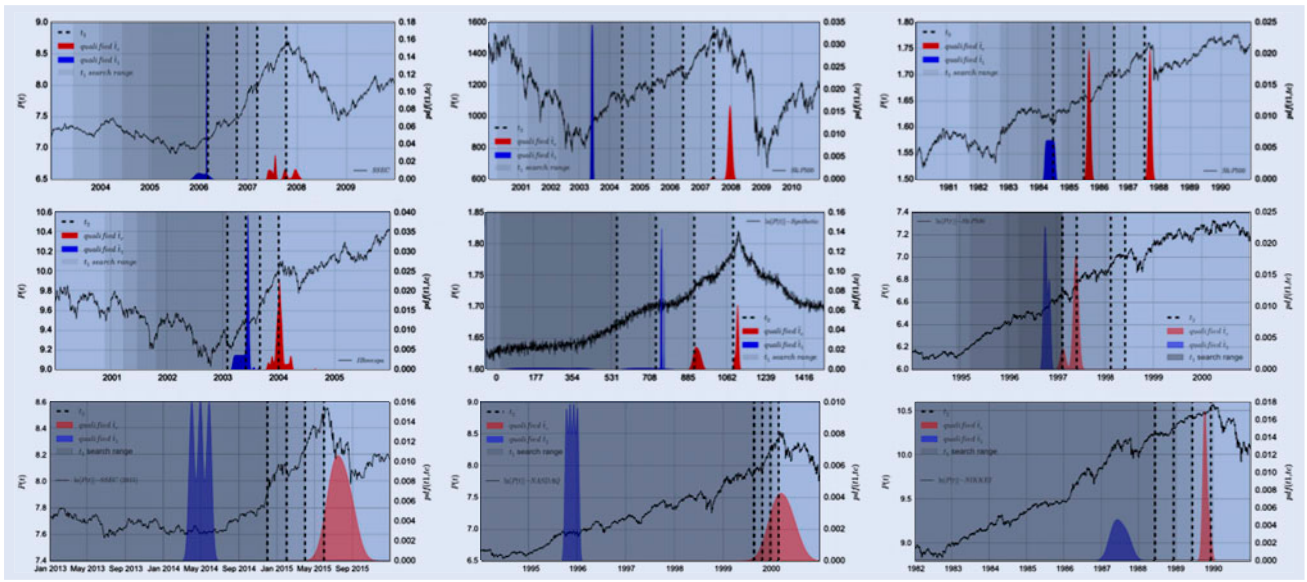

Figure 8. Analysis of the eight bubbles described in section 3.1 as well as for a synthetic bubble, for four different values of t_2 shown by the vertical dashed black lines in each panel. The red (resp. blue) filled curve represents the pdf of $\widehat{t_c^*}$ (resp. $\widehat{t_1^*}$) over the set of time windows obtained from the four t_2's by scanning t_1 over their corresponding grey shaded area, each of the same width of 600 days. The pdf's are represented using a kernel method with bandwidth ≈ 0.1 year.

ing the original cost function (A6) without t_1. Applying the standard unit-root Augmented Dickey–Fuller and Phillips–Perron tests to the residuals of the best fits confirms that they are mean-reversing, in agreement with the condition proposed by Lin *et al.* (2014) (see table 5 and figure 9 in the Supplementary Materials). Figure 4 shows the same ellipse-shaped structure as obtained previously in our synthetic tests described in section 2.6 and the same order of the importance of the parameters m, ω, t_1 and t_c associated, respectively, from the largest eigenvalue to the smallest one. This structure is also robust when using the LPPLS cost function without t_1 as a parameter to calibrate (see table 4).

The dependence of the cost function $\chi^2(\Phi)$ for the same eight studied empirical bubbles along the three different pairs of parameters (t_1, m), (t_1, ω) and (t_1, t_c) is shown in figure 5. One can observe a much more complicated landscape than

Table 3. Hessian matrix, eigenvalues and corresponding eigenvectors for the best LPPLS fits using equation (4) of the financial bubbles described in section 3.1 in the time windows $[t_1^* : t_2]$ given in the table for each bubble. The numbers in boldface indicate the parameters that contribute the most to their eigenvectors.

	Hessian, H(Φ^*)					Eigenvectors, $\vec{v}$			
	m	ω	t_c	t_1	$\lambda/\lambda_{\max}$	m	ω	t_c	t_1
S&P 500 (1997)									
	$t_1^* \approx$ July 1996, $t^2 \approx$ February 1997								
m	1.98e−1				1.00e0	**−9.66e−1**	−2.58e−1	−6.15e−5	−7.89e−3
ω	3.85e−2	6.40e−2			2.60e−1	−2.57e−1	**9.61e−1**	4.34e−4	1.00e−1
t_c	9.31e−6	9.77e−6	1.03e−4		2.05e−2	1.82e−2	−9.88e−2	3.91e−2	**9.94e−1**
t_1	2.65e−4	5.23e−3	1.65e−4	4.78e−3	4.63e−4	−6.63e−4	3.43e−3	**9.99e−1**	−3.90e−2
SSEC (2015)									
	$t_1^* \approx$ March 2014, $t^2 \approx$ June 2015								
m	6.55e−1				1.00e0	**−9.80e−1**	−1.98e−1	−3.94e−3	−7.08e−4
ω	1.25e−1	6.40e−2			5.68e−2	−1.98e−1	**9.79e−1**	−1.38e−2	3.59e−2
t_c	2.74e−3	8.25e−6	7.53e−5		5.73e−3	6.39e−3	−3.5e−2	7.76e−3	**9.99e−1**
t_1	2.21e−4	1.32e−3	1.25e−5	3.95e−3	8.38e−5	6.67e−3	−1.30e−2	**−9.99e−1**	7.26e−3
NASDAQ									
	$t_1^* \approx$ January 1996, $t^2 \approx$ February 2000								
m	9.07e−1				1.00e0	**−9.93e−1**	−1.12e−1	−8.27e−4	−1.01e−2
ω	1.01e−1	2.55e−2			1.53e−2	−1.12e−1	**9.92e−01**	−6.00e−03	5.01e−2
t_c	7.65e−4	2.05e−7	4.01e−6		7.56e−4	4.52e−3	5.07e−2	−3.45e−2	**−9.98e−1**
t_1	9.22e−3	1.72e−3	2.74e−5	8.23e−4	2.22e−6	1.34e−3	−7.62e−3	**−9.99e−1**	3.42e−02
NIKKEI									
	$t_1^* \approx$ January 1988, $t^2 \approx$ December 1989								
m	9.20e−1				1.00e0	**−9.99e−1**	−4.40e−2	−9.73e−5	−4.38e−4
ω	4.05e−2	3.70e−3			2.07e−3	−4.40e−2	**9.98e−1**	−2.05e−3	−1.80e−2
t_c	8.98e−5	2.02e−8	5.12e−7		1.07e−3	1.23e−3	−1.80e−2	8.76e−5	**−9.99e−1**
t_1	4.04e−4	1.07e−6	2.40e−8	9.87e−4	5.37e−7	1.87e−4	−2.05e−3	**−9.99e−1**	−5.04e−5

in figure 4 with multiple local minima associated with the introduction of the parameter t_1. Figure 5 demonstrates that the normalized cost function exhibits an overall decrease as t_1 increases, because the calibration has a smaller number of degrees of freedom to explain for smaller $t_2 - t_1$. This tends to bias the estimation of t_1 upward, i.e. to underestimate the true duration of the bubble. Figures 5 and 6 exemplify that t_c has very little impact on the value of $\chi^2(\Phi)$ once t_1 is given. In other words, one can really visualize here the sloppiness of t_c compared with the relatively much larger rigidity of t_1. This feature is absent for the pairs (t_1, m) and (t_1, ω), as small changes in m and ω often lead to significant variations of the cost function, in agreement with the information contained in the corresponding eigenvalues. One can also observe that, for certain values of t_1, the cost function exhibits clear minima as a function of t_c, supporting previous claims that the end of financial bubbles may be predictable only at certain time intervals, i.e. in 'pockets of predictability' (Sornette and Cauwels 2015).

3.3. *Visualization of the relative rigidity of t_1 vs. the slopiness of t_c using their pdf's*

The stability of t_1 relative to t_c for the eight empirical bubbles described in section 3.1 is visualized in figure 7. For a given $\bar{t}_2$ (black vertical dashed line in each panel), the blue filled function represents the pdf of the qualified calibrated $\widehat{t}_1^*$'s in a search over the grey interval up to $\bar{t}_2 - 30$ days. The red filled function represents the corresponding pdf of qualified calibrated $\widehat{t}_c^*$'s. It is pleasant to observe that the pdf of $\widehat{t}_1^*$ is where one would visually locate a priori the start of the bubble, as this is the time when the price starts to present evidence of a faster-than-exponential growth. The pdf of $\widehat{t}_c^*$ is not too far from the true time of the change of regime but is often too late, except for the bubble on the IBovespa index.

The sensitivity analysis performed around the best solution of $\widehat{t}_1^*$ and $\widehat{t}_c^*$ demonstrates that t_1 is even more important than t_c for the calibration, relative to the study performed on synthetic data. Specifically, changes in t_1 lead to fluctuations of the

Table 4. Hessian matrix, eigenvalues and corresponding eigenvectors for the best LPPLS fits for the four studied empirical bubbles described in section 3.1 using equation (A6). The numbers represented in boldface identify the parameters that contribute most to their corresponding eigenvalue.

	Hessian H(ϕ^*)				Eigenvectors $\vec{v}$		
	m	ω	t_c	λ/λ_{max}	m	ω	t_c
SSEC							
$t_1^* \approx$ February 2005, $t^2 \approx$ October 2007							
m	1.46e−1			1.00e0	**9.99e−1**	2.32e−2	1.24e−4
ω	3.32e−3	3.41e−3		2.28e−2	2.31e−2	9.98e−1	4.62e−2
t_c	1.46e−5	1.55e−4	1.00e−5	1.93e−5	9.49e−4	4.62e−2	9.98e−1
S&P500 (SP)							
$t_1^* \approx$ December 2003, $t^2 \approx$ July 2007							
m	1.21e−2			1.00e0	9.99e−1	3.15e−2	1.80e−3
ω	3.46e−4	1.22e−3		9.95e−2	3.15e−2	9.99e−1	2.54e−2
t_c	2.10e−5	3.15e−5	8.98e−7	5.81e−6	9.98e−4	2.55e−2	9.99e−1
S&P500 (BM)							
$t_1^* \approx$ March 1984, $t^2 \approx$ August 1987							
m	3.24e−1			1.00e0	9.99e−1	4.07e−2	3.02e−3
ω	1.22e−2	2.54e−2		7.70e−2	4.08e−2	9.98e−1	4.56e−2
t_c	9.33e−4	1.10e−3	1.71e−3	5.12e−3	1.16e−3	4.57e−2	9.98e−1
IBovespa							
$t_1^* \approx$ June 2003, $t^2 \approx$ January 2004							
m	1.21e−2			1.00e0	9.83e−1	1.81e−1	−8.095009e−03
ω	1.80e−3	2.67e−3		1.88e−1	1.80e−1	9.82e−1	4.578182e−02
t_c	1.17e−4	8.36e−5	9.23e−5	6.96e−3	1.62e−2	4.35e−2	9.989187e−01
S&P500 (1997)							
$t_1^* \approx$ July 1996, $t^2 \approx$ February 1997							
m	9.16e−4			1.00e0	**9.99e−1**	3.12e−2	1.33e−2
ω	2.62e−5	6.83e−5		7.86e−2	3.35e−2	**9.98e−1**	2.55e−1
t_c	1.16e−5	−1.77e−5	6.72e−6	2.15e−3	2.15e−3	2.56e−1	**9.66e−1**
SSEC (2015)							
$t_1^* \approx$ March 2014, $t^2 \approx$ June 2015							
m	1.57e−1			1.00e0	9.99e−1	3.67e−2	4.09e−3
ω	5.55e−3	6.71e−3		4.13e−2	3.69e−2	9.98e−1	4.58e−2
t_c	6.34e−4	3.17e−4	1.25e−4	6.95e−4	2.39e−3	4.60e−2	9.98e−1

(*continued*)

Table 4. (*Continued*).

NASDAQ							
$t_1^* \approx$ January 1996, $t^2 \approx$ February 2000							
	Hessian H(ϕ^*)				**Eigenvectors $\vec{v}$**		
	m	ω	t_c	$\lambda/\lambda_{\max}$	m	ω	t_c
m	4.11e−1			1.00e0	9.99e−1	1.65e−2	1.27e−3
ω	6.46e−3	2.13e−2		5.14e−2	1.65e−2	9.99e−1	1.43e−2
t_c	5.19e−4	3.13e−4	5.44e−6	9.39e−7	1.03e−3	1.44e−2	9.99e−1
NIKKEI							
$t_1^* \approx$ January 1988, $t^2 \approx$ December 1989							
	Hessian H(ϕ^*)				Eigenvectors $\vec{v}$		
	m	ω	t_c	$\lambda/\lambda_{\max}$	m	ω	t_c
m	8.72e−4			1.00e0	9.85e−1	1.68e−1	4.14e−3
ω	1.30e−4	1.32e−4		1.23e−1	1.69e−1	9.85e−1	−1.87e−2
t_c	−3.30e−6	−2.65e−6	5.44e−8	4.48e−7	9.21e−4	1.91e−2	9.99e−1

Table 5. Diagnosis of the LPPLS fits with calibrated parameters Φ^* for the four studied empirical bubbles described in section 3.1 and one synthetic data. We easily reject the hypothesis that the residuals are unit-root at the 99% confidence level. Values in brackets give the *p-values* of the test statistic.

				AR(1) residuals ($\vec{r}$) test	
Index	Damping	Number of oscillations	LPPLS conditions	Dickey–Fuller	Phillips–Perron
Synthetic LPPLS	3.36	5.27	Satisfied	−3.420 (10^{-3})	−3.610 (10^{-3})
SSEC	1.04	3.91	Satisfied	−4.653 (10^{-3})	−4.642 (10^{-3})
S&P 500(*SP*)	1.15	5.13	Satisfied	−4.710 (10^{-3})	−4.702 (10^{-3})
S&P 500(*BM*)	1.41	4.02	Satisfied	−3.641 (10^{-3})	−3.641 (10^{-3})
IBovespa	1.85	3.47	Satisfied	−4.620 (10^{-3})	−4.610 (110^{-3})
S&P 500(1997)	1.15	2.32	Satisfied	−4.710 (10^{-3})	−4.702 (10^{-3})
SSEC (2015)	1.39	2.86	Satisfied	−4.710 (10^{-3})	−4.702 (10^{-3})
NASDAQ	1.32	2.63	Satisfied	−4.710 (10^{-3})	−4.702 (10^{-3})
NIKKEI	1.03	2.51	Satisfied	−4.710 (10^{-3})	−4.702 (10^{-3})

normalized sum of squared residuals spanning the interval (−2.0% to 2.0%), (0.0% to 1.0%), (−0.5% to 1.0%), (−2.0% to 2.0%), (0.0% to 1.75%), (0.0% to 2.5%), (0.0% to 2.0%), (0.0% to 3.0%), respectively, for the SSEC, SP, BM and IBovespa, SP-1997, SSEC-2015, NASDAQ and NIKKEI bubbles. In contrast, changes in t_c have negligible impact on the cost function.

Even accounting for their errors bars, one can observe that λ_3 is at least two orders of magnitude larger that λ_4 for all t_1's, corroborating the results of section 2.7. The parameters t_1 and t_c contribute, respectively, to λ_3 and λ_4 more than 35% throughout the analysed periods. Taken together, these features strengthen the evidence of the greater sloppiness of t_c compared to t_1, which makes the determination of the end of bubbles much more difficult that their beginning.

Finally, it is important to check how the above results generalize for different 'present' times t_2, mimicking a real-time situation of a developing bubble. As seen in figure 8, we consider four different values of t_2 shown by the vertical dashed black lines in each panel. Note that these four choices cover most of the duration of the bubbles. For each t_2, we search the optimal t_1 that minimizes the cost function up to 600 days prior t_2. This intervals in which t_1 is scanned are represented by the different shades of grey, one per value of t_2.

One can observe that the pdf's of $\widehat{t_c^*}$ are quite wide and with several modes, except for the bubble on the S&P500 that burst in 2007. These modes are localized at times when the markets corrected, in addition to finding a neighbourhood of the true ends of the bubbles. In contrast, the pdf's of $\widehat{t_1^*}$ are monomodal, very narrow and pinpoint a time when the markets start their significant ascent. For instance, for the *S&P*500 Index during the 1980s, our analysis identifies two possible modes for the end of the bubble, one occurring in the last quarter of 1985 associated with a significant drawdown and the other being close to the crash on 19 October 1987. Conversely, the narrow pdf of $\widehat{t_1^*}$ identifies the beginning of the bubble around mid-1984. A similar situation is observed for the SSEC Index as well as for the synthetic case.

The existence of several modes of the pdf's of $\widehat{t_c^*}$ can be traced to the discrete scale invariance of the log-periodic oscillations (Sornette 1998), associated with the occurrence of corrections or plateaux decorating the super-exponential growth, each of them being interpreted as a possible candidate for the end of the bubble by the calibration procedure. When used to diagnose bubbles, this confirms that the LPPLS model can determine t_1 significantly more accurately than t_c.

4. Conclusion

We have presented systematic tests of the precision and reliability with which the beginning and end of a bubble can be determined. This has required using a specific bubble model, the LPPLS model, which represents a bubble as a transient noisy super-exponential price trajectory augmented by accelerated volatility oscillations. One of the quality of the LPPLS model is to contain the end time t_c of the bubble as a defining parameter, which can thus be estimated over various time windows. In order to estimate the beginning of a bubble, we have proposed to endogenize in the cost function the parameter t_1 defining the beginning of the time window that provides the best goodness of fit and satisfies the LPPLS model conditions. The cost function quantifying the quality of fit of the LPPLS model has been extended to include t_1. Using the Fisher Information matrix, we have quantified the parameter uncertainty associated with the determination of both t_1 and t_c. Using both synthetic data and eight historical bubble cases, we find overwhelming evidence that the beginning of bubbles is much better constrained that their end. This is quantified by calculating the eigenvalues of the Hessian matrix, which characterize the shape of the cost function in the different directions in parameter space. Parameters associated with large eigenvalues are 'rigid', i.e. they tend to be well estimated. In contrast, parameters associated with small eigenvalues are 'sloppy', as large changes of their values do not impact the cost function, which is degenerate along their directions in parameter space. We find that the eigenvalues for which t_1 contributes most are several order of magnitudes larger than the eigenvalues for which t_c contributes most. Practically, this implies that the beginning of financial bubbles are comparatively much easier to determine using LPPLS than their ending time t_c. Our results are robust over all eight empirical bubbles and many synthetic tests, as well as when changing the time t_2 (the 'present') of analysis.

Building on the initial sloppy-rigid analysis of the LPPLS model performed by Bree *et al*. (2013), our results corroborate their findings regarding the sloppiness of t_c. Moreover, we propose an answer to the open question regarding beginning of financial bubbles. Our results are also confirm those obtained by Lin *et al*. (2014) when studying the beginning of Black-Monday bubble of 1987. Finally, our analysis gives support to the empirical evidence among practitioners (in particular hedge-funds (Gurkaynak 2008)), who tend to correctly diagnose ongoing bubbles but in general fail to time their end.

As a side result, we have found that two structural parameters of the LPPLS model, the exponent m controlling the super-exponential growth of price and the angular log-periodic frequency ω describing the log-periodic acceleration of volatility, are very rigid. This suggests that the LPPLS model is a reasonable candidate for describing the generating process of prices during bubbles (Sornette 2003).

Finally, contrary to the claim in the literature that bubbles are not suppressed by arbitrageurs because they fail to agree on the beginning of the bubble (Abreu and Brunnermeier 2003), our findings suggests that bubbles persist due to the difficulty of synchronizing opinions on the end of bubbles.

Acknowledgements

The authors would like to acknowledge V. Filimonov. All calculations and figures were elaborated using open source software IPython (Pérez and Granger 2007). The authors would like to thank the editor and two anonymous referees.

Disclosure statement

No potential conflict of interest was reported by the authors.

Funding

This work was partially supported by CNPq (Conselho Nacional de Desenvolvimento Científico e Tecnológico) [grant number FP7-319968].

Supplemental data

Supplemental data for this article can be accessed at http://dx.doi/10.1080/14697688.2016.1231417.

References

Abreu, D. and Brunnermeier, M.K., Bubbles and crashes. *Econometrica*, 2003, **71**, 173–204.

Bak, P., Tang, C. and Wiesenfeld, K., Self-organized criticality. *Phys. Rev. A*, 1988, **3**, 364–374.

Barberis, N., Shleifer, A. and Vishny, R., A model of investor sentiment. *J. Financ. Econ.*, 1998, **49**, 307–343.

Blanchard, O.J. and Watson, M.W., Bubbles, rational expectations and financial markets. Working Paper 945, National Bureau of Economic Research, 1982.

Bree, D., Challet, D. and Peirano, P., Prediction accuracy and sloppiness of log-periodic functions. *Quant. Finance*, 2013, **3**, 275–280.

Brown, K.S. and Sethna, J.P., Statistical mechanical approaches to models with many poorly known parameters. *Phys. Rev. E*, 2003, **68**, 021904.

Brunnermeier, M.K. and Nagel, S., Hedge funds and the technology bubble. *J. Finance*, 2004, **59**, 2013–2040.

Filimonov, V. and Sornette, D., A stable and robust calibration scheme of the log-periodic power law model. *Physica A*, 2013, **17**, 3698–3707.

Geraskin, P. and Fantazzini, D., Everything you always wanted to know about log-periodic power laws for bubble modeling but were afraid to ask. *Eur. J. Finance*, 2011, **19**, 366–391.

Graf v. Bothmer, H.C. and Meister, C., Predicting critical crashes? A new restriction for the free variables. *Physica A*, 2003, **320**, 539–547.

Gurkaynak, R., Econometric tests of asset price bubbles: Taking stock. *J. Econ. Surv.*, 2008, **22**, 166–186.

Harrison, M. and Kreps, D.M., Speculative investor behavior in a stock-market with heterogeneous expectations. *Q. J. Econ.*, 1978, **92**, 323–336.

Huang, Y., Johansen, A., Lee, M.W., Saleur, H. and Sornette, D., Artifactual log-periodicity in finite-size data: Relevance for earthquake aftershocks. *J. Geophys. Res.*, 2000, **105**, 25451–25471.

Hüsler, A., Sornette, D. and Hommes, C.H., Super-exponential bubbles in lab experiments: Evidence for anchoring over-optimistic expectations on price. *J. Econ. Behav. Organiz.*, 2012, **92**, 304–316.

Jiang, Z.Q., Zhou, W.X., Sornette, D., Woodard, R., Bastiaensen, K. and Cauwels, P., Bubble diagnosis and prediction of the 2005–2007 and 2008–2009 Chinese stock market bubbles. *J. Econ. Behav. Organiz.*, 2010, **74**, 149–162.

Johansen, A., Ledoit, O. and Sornette, D., Crashes as critical points. *Int. J. Theor. Appl. Finance*, 2000, **2**, 219–255.

Johansen, A. and Sornette, D., Shocks, crashes and bubbles in financial markets. *Brussels Econ. Rev. (Cahiers economiques de Bruxelles)*, 2010, **53**, 201–253.
Kaizoji, T. and Sornette, D., Market bubbles and crashes. In *Encyclopedia of Quantitative Finance*, 2010 (Wiley). Long version available online at: http://arXiv.org/abs/0812.2449.
Kindleberger, C.P., *Manias, Panics and Crashes: A History of Financial Crises*, Vol. 3, 1978 (Macmillan: London).
Lin, L., Ren, R.E. and Sornette, D., The volatility-confined LPPL model: A consistent model of 'explosive' financial bubbles with mean-reverting residuals. *Int. Rev. Financ. Anal.*, 2014, **33**, 210–222.
Machta, B., Chachra, R., Transtrum, M. and Sethna, J., Parameter space compression underlies emergent theories and predictive models. *Science*, 2013, **342**, 604–607.
Marquardt, D., An algorithm for least-squares estimation of nonlinear parameters. *SIAM J. Appl. Math.*, 1962, **2**, 431–441.
Minsky, H.P., The modeling of financial instability: An introduction. In *Proceedings of the Fifth Annual Pittsburgh Conference*, New York, 1974.
Pérez, F. and Granger, B.E., IPython: A system for Interactive Scientific Computing. *Comput. Sci. Eng.*, 2007, **9**, 21–29.
Saleur, H. and Sornette, D., Complex exponents and log-periodic corrections in frustrated systems. *J. Phys. I France*, 1996, **6**, 327–355.
Samuelson, P., Proof that properly anticipated prices fluctuate randomly. *Ind. Manage. Rev.*, 1965, **6**, 41–49.
Shiller, R.J., Do stock prices move too much to be justified by subsequent changes in dividends? *Am. Econ. Rev.*, 1981, **71**, 421–436.
Shiller, R., *Irrational Exuberance*, 2000 (Princeton University Press: Princeton, NJ).
Shleifer, A., *Inefficient Markets: An Introduction to Behavioral Finance*, Clarendon Lectures in Economics, 2000 (Oxford University Press: Princeton, NJ).
Sornette, D., Discrete scale invariance and complex dimensions. *Phys. Rep.*, 1998, **297**, 239–270. Extended version available online at: http://xxx.lanl.gov/abs/cond-mat/9707012.
Sornette, D., *Why Stock Markets Crash: Critical Events in Complex Financial Systems*, 2003 (Princeton University Press: Princeton, NJ).
Sornette, D., Physics and financial economics (1776—2014): Puzzles, ising and agent-based models. *Rep. Prog. Phys.*, 2014, **77**, 062001.
Sornette, D. and Cauwels, P., 1980–2008: The illusion of the perpetual money machine and what it bodes for the future. *Risks*, 2014, **2**, 103–131.
Sornette, D. and Cauwels, P., Financial bubbles: Mechanisms, diagnostics and state of the world. *Rev. Behav. Econ.*, 2015, **2**, 279–305.
Sornette, D. and Johansen, A., Significance of log-periodic precursors to financial crashes. *Quant. Finance*, 2001, **1**, 452–471.
Sornette, D., Demos, G., Zhang, Q., Cauwels, P., Filimonov, V. and Zhang, Q., Real-time prediction and post-mortem analysis of the Shanghai 2015 stock market bubble and crash. *J. Invest. Strat.*, 2015, **4**, 77–95.
Sornette, D., Johansen, A. and Bouchaud, J.P., Stock market crashes, precursors and replicas. *J. Phys.*, 1995, **6**, 167–175.
Sornette, D. and Woodard, R., Financial bubbles, real estate bubbles, derivative bubbles, and the financial and economic crisis (2009). In *Proceedings of APFA7 (Applications of Physics in Financial Analysis), 'Econophysics Approaches to Large-Scale Business Data and Financial Crisis'*, edited by M. Takayasu, T. Watanabe and H. Takayasu, pp. 101–148, 2010 (Springer: Berlin).
Transtrum, M.K., Machta, B.B. and Sethna, J.P., Geometry of nonlinear least squares with applications to sloppy models and optimization. *Phys. Rev. E*, 2011, **83**, 673–701.
Transtrum, M. and Sethna, J., Improvements to the Levenberg–Marquardt algorithm for nonlinear least-squares minimization, arXiv preprint, 2012. Available online at: http://arxiv.org/abs/1201.5885.
Tsay, R., *Analysis of Financial Time-series*, Vol. 3, Wiley Series in Probability and Statistics, 2010 (Wiley: New York).
Xiong, W., Bubbles, crisis and heterogeneous beliefs. In *Handbook on Systemic Risk*, edited by J.-P. Fouque and J.A. Langsam, Chapter 24, pp. 663–713, 2013 (Cambridge University Press: Princeton, NJ).

Appendix 1. Calibration of the LPPLS model (3)

We use the formulation in terms of the four linear parameters A, B, C_1, C_2 and three nonlinear parameter m, ω, t_c (Filimonov and Sornette 2013), so that the log-price given by expression (3) can be written as

$$fLPPL(\boldsymbol{\phi}, t) = A + B(f) + C_1(g) + C_2(h), \tag{A1}$$

where $\boldsymbol{\phi} = \{A, B, C_1, C_2, m, \omega, t_c\}$ is a (1×7) vector of parameters we want to determine and

$$f \equiv (tc - t)^m, \tag{A2}$$
$$g \equiv (t_c - t)^m \cos(\omega \ln(t_c - t)), \tag{A3}$$
$$h \equiv (t_c - t)^m \sin(\omega \ln(tc - t)). \tag{A4}$$

Let $y := \vec{P} = [p_1, p_2, \ldots, p_N]$ denote a price realization vector consisting of N observations and the discrete time vector $t = [1, 2, \ldots, N]$. Fitting equation (A1) to the logarithm of $\vec{P}$ amounts to search for the parameter set $\boldsymbol{\phi}^*$ that yields the smallest N-*dimensional* distance between realization and theory. Mathematically, using the L^2 norm, we form the following sum of squares of residuals

$$F(t_c, m, \omega, A, B, C_1, C_2) = \sum_{i=1}^{N} \Big[\ln[P(t_i)] - A - B(f_i) - C_1(g_i) - C_2(h_i)\Big]^2, \tag{A5}$$

for $i = 1, \ldots, N$. We proceed in two steps. First, slaving the linear parameters $\{A, B, C_1, C_2\}$ to the remaining nonlinear parameters $\boldsymbol{\phi} = \{t_c, m, \omega\}$, yields the cost function $\chi^2(\boldsymbol{\phi})$

$$\chi^2(\boldsymbol{\phi}) := F_1(t_c, m, \omega) = \min_{\{A,B,C_1,C_2\}} F(t_c, m, \omega, A, B, C_1, C_2) = F(t_c, m, \omega, \widehat{A}, \widehat{B}, \widehat{C}_1, \widehat{C}_2), \tag{A6}$$

where the hat symbol $\widehat{\ }$ indicates estimated parameters. This is obtained by solving the optimization problem

$$\{\widehat{A}, \widehat{B}, \widehat{C}_1, \widehat{C}_2\} = arg \min_{\{A,B,C_1,C_2\}} F(t_c, m, \omega.A, B, C_1, C_2), \tag{A7}$$

which can be obtained analytically by solving the following matrix equations

$$\begin{bmatrix} N & \sum f_i & \sum g_i & \sum h_i \\ \sum f_i & \sum f_i^2 & \sum f_i g_i & \sum f_i h_i \\ \sum g_i & \sum f_i g_i & \sum g_i^2 & \sum g_i h_i \\ \sum h_i & \sum f_i h_i & \sum g_i h_i & \sum h_i^2 \end{bmatrix} \begin{bmatrix} \widehat{A} \\ \widehat{B} \\ \widehat{C}_1 \\ \widehat{C}_2 \end{bmatrix} = \begin{bmatrix} \sum y_i \\ \sum y_i f_i \\ \sum y_i g_i \\ \sum y_i h_i \end{bmatrix} \tag{A8}$$

Second, we solve the nonlinear optimization problem involving the remaining nonlinear parameters m, ω, t_c:

$$\{\widehat{t_c}, \widehat{m}, \widehat{\omega}\} = arg \min_{\{t_c,m,\omega\}} F_1(t_c, m, \omega). \tag{A9}$$

Appendix 2. Calibration of the extended set of four non-linear parameters $\Phi = \{m, \omega, t_c, t_1\}$

We compute the first-order partial derivatives of equation (4)—i.e. the Gradient vector $\vec{\nabla}\chi^2(\boldsymbol{\Phi})$—with respect to each parameter as follows:

$$\begin{aligned}
&\frac{\partial \chi^2(\Phi)}{\partial m} \\
&= \frac{2\ln(t_c - t)(t_c - t)^m\,[\,\sin(\ln(t_c - t)\,\omega) + \cos(\ln(t_c - t)\omega) - B\,]}{t_2 - t_1} \\
&\quad \times \frac{[\,(t_c - t)^m\,\sin(\ln(t_c - t)\,\omega + \cos(\ln(t_c - t)\omega) - B)}{t_2 - t_1} \\
&\quad + \frac{C_1 + C_2 + A\,]}{t_2 - t_1}
\end{aligned} \tag{B1}$$

$$\begin{aligned}
&\frac{\partial \chi^2(\Phi)}{\partial \omega} \\
&= \frac{-2\ln(t_c - t)(t_c - t)^m\,[\,\sin(\ln(t_c - t)\,\omega - \cos(\ln(t_c - t)\omega)\,])}{t_2 - t_1} \\
&\quad \times \frac{[\,(t_c - t)^m\,\sin(\ln(t_c - t)\,\omega + \cos(\ln(t_c - t)\omega) - B)}{t_2 - t_1} \\
&\quad + \frac{C_1 + C_2 + A\,]}{t_2 - t_1}
\end{aligned} \tag{B2}$$

$$\begin{aligned}
&\frac{\partial \chi^2(\Phi)}{\partial t_c} \\
&= \frac{-2(t_c - t)^{m-1}\,[\,(C_1\omega - C_2 m)\,\cos(\omega\ln(t_c - t)) + Bm)(t_c - t)^m}{t_2 - t_1} \\
&\quad \times \frac{(C_2\sin(\omega\ln(t_c - t)) + C_1\cos(\omega\ln(t_c - t))}{t_2 - t_1} \\
&\quad + \frac{-B) + A]}{t_2 - t_1}
\end{aligned} \tag{B3}$$

$$\begin{aligned}
&\frac{\partial \chi^2(\Phi)}{\partial t_1} \\
&= \frac{(-y + C_2(t_c - t)^m\,\sin(\ln(t_c - t)\omega) + C_1(t_c - t)^m\,\cos(\ln(t_c - t)\omega)}{(t_2 - t_1)^2} \\
&\quad + \frac{B(t_c - t)^m + A)^2}{(t_2 - t_1)^2}.
\end{aligned} \tag{B4}$$

These first-order partial derivatives are collected by the Jacobian matrix $J(\boldsymbol{\Phi})_{(N\times m)}$,

$$J(\boldsymbol{\Phi}) = \begin{bmatrix} \frac{\partial r_i}{\partial \Phi_i} \\ \vdots \\ \frac{\partial r_i}{\partial \Phi_j} \end{bmatrix} \equiv \begin{bmatrix} \frac{\partial r_i}{\partial m}\ \frac{\partial r_i}{\partial \omega}\ \frac{\partial r_i}{\partial t_c}\ \frac{\partial r_i}{\partial t_1} \end{bmatrix}^{\mathsf{T}}_{\substack{j=1,2,\ldots,m; \\ i=1,2,\ldots,N;}}, \tag{B5}$$

where $r_i(\boldsymbol{\Phi}) = y(t)_i - flppl(\boldsymbol{\Phi}, t)_i$ are defined in equation (4).

Embedded within a m-dimensional Euclidean space, the Gradient vector points towards directions in which the cost increases more rapidly. At a given local minimum, the minimization problem should not only display small $\vec{\nabla}\chi^2(\boldsymbol{\Phi})$ values but also, the cost curvature should be convex and the residuals approximately zero. Formally, this idea is expressed as

$$\Delta\chi^2(\boldsymbol{\Phi}) = \frac{1}{2}\vec{\nabla}(\boldsymbol{\Phi})^{\mathsf{T}}\boldsymbol{H}(\boldsymbol{\Phi}^*)\vec{\nabla}(\boldsymbol{\Phi}) \geq 0, \tag{B6}$$

where $\boldsymbol{H}(\boldsymbol{\Phi}^*)$ denotes the Hessian matrix expressed at the best-fit parameters. Bold letters denote either matrices or vectors. This special structure of the sum of squares of residuals allows one to approximate $\boldsymbol{H}(\boldsymbol{\Phi}^*)$ in terms of the fitting residuals using,

$$\frac{\partial \chi^2(\boldsymbol{\Phi})}{\partial \Phi_i \Phi_j} = \sum_{i=1}^{m}\left(r_i\frac{\partial^2 r_i(\Phi)}{\partial \Phi_i \partial \Phi_j} + \frac{\partial r_i(\Phi)}{\partial \Phi_i}\frac{\partial r_i(\Phi)}{\partial \Phi_j}\right). \tag{B7}$$

Since equation (B6) holds, we therefore skip the calculation of second-order derivatives and compute $\boldsymbol{H}(\boldsymbol{\Phi}^*)$ solely using the Jacobian (Tsay 2010, Machta *et al*. 2013),

$$\boldsymbol{H}|_* \equiv \boldsymbol{J}^{\mathsf{T}}\boldsymbol{J} = \sum_{i=1}^{N}(\vec{\nabla}r_i(\boldsymbol{\Phi}^*))(\vec{\nabla}r_j(\boldsymbol{\Phi}^*))^{\mathsf{T}}. \tag{B8}$$

At the best-fit, the Hessian is always *symmetric*, positive-definite and has entries according to

$$H_{i,j}^{\chi^2(\Phi^*)} = \begin{bmatrix} \frac{\partial^2 r_i(\Phi)}{\partial m,\partial m} & \frac{\partial^2 r_i(\Phi)}{\partial m,\partial \omega} & \frac{\partial^2 r_i(\Phi)}{\partial m,\partial t_c} & \frac{\partial^2 r_i(\Phi)}{\partial m,\partial t_1} \\ \frac{\partial^2 r_i(\Phi)}{\partial \omega,\partial m} & \frac{\partial^2 r_i(\Phi)}{\partial \omega,\partial \omega} & \frac{\partial^2 r_i(\Phi)}{\partial \omega,\partial t_c} & \frac{\partial^2 r_i(\Phi)}{\partial \omega,\partial t_1} \\ \frac{\partial^2 r_i(\Phi)}{\partial t_c,\partial m} & \frac{\partial^2 r_i(\Phi)}{\partial t_c,\partial \omega} & \frac{\partial^2 r_i(\Phi)}{\partial t_c,\partial t_c} & \frac{\partial^2 r_i(\Phi)}{\partial t_c,\partial t_1} \\ \frac{\partial^2 r_i(\Phi)}{\partial t_1,\partial m} & \frac{\partial^2 r_i(\Phi)}{\partial t_1,\partial \omega} & \frac{\partial^2 r_i(\Phi)}{\partial t_1,\partial t_c} & \frac{\partial^2 r_i(\Phi)}{\partial t_1,\partial t_1} \end{bmatrix}. \tag{B9}$$

Derivatives are calculated using a *centred finite-difference scheme*,

$$\chi^2(\boldsymbol{\Phi}^*)' \approx \frac{\chi^2(\boldsymbol{\Phi}^* + h) - \chi^2(\boldsymbol{\Phi}^* - h)}{2h}, \tag{B10}$$

with step-size h varying according to information provided by the Gradient. The choice of h should neither be too small or too large.